A Frequency Offset Transmit Reference System in Dense Multipath Environments: Propagation Effects and Design Considerations

Ibrahim Bilal, Arjan Meijerink, *Senior Member, IEEE*, and Mark J. Bentum, *Senior Member, IEEE*

***Abstract*— Frequency offset transmit reference (FoTR)—a noncoherent spread spectrum technique—is considered in dense multipath fading environments, in the context of wideband communication. The interplay between system parameters and propagation effects is investigated. Analytical relations between key design parameters and the channel delay spread are derived, which provide a framework for determining reasonable system parameters that optimize the performance. An approximated closed-form expression for the outage probability is also obtained, which is shown to be fairly accurate for low outage probabilities. It is shown that FoTR suffers significantly from noise-enhancement, but, is nonetheless, robust against frequency-selective fading. A large value of frequency offset can significantly deteriorate the performance, particularly in environments with large channel delay spreads. This restricts the maximum data rate as well as the multiple-access capability of the scheme. Despite the limitations, FoTR can be a useful communication scheme for low data rate sensor networks deployed in dense multipath environments, particularly where the design demands a simple receiver and a low outage probability.**

***Index Terms*— Low-power radios, noise-based communication, outage probability, propagation effects, spread spectrum, transmit reference, wireless sensor networks.**

I. Introduction

DIRECT-sequence spread spectrum (DSSS) communication is an attractive choice for wireless sensor networks (WSNs), mainly due to its resistance to narrowband interference, immunity to channel impairments, and good multiple access (MA) capability. In most sensor applications, the communication usually experiences non-line-of-sight (NLOS) propagation environments, where the transmitted signal is scattered. To collect most of the transmitted energy, a coherent DSSS receiver is typically implemented, which decodes the signal received from each multipath component (MPC), and combines them intelligently to improve the quality of the recovered signal. This well-known *rake* receiver demands precise synchronization and accurate channel knowledge, and its architectural complexity increases with increasing operational bandwidth. In monitoring applications, where the transmissions are sporadic, the coherent DSSS receiver is an unsuitable choice. The traffic is bursty in nature, and for such applications, the channel estimation and synchronization for each burst of data is power-inefficient.

In an attempt to avoid the complexity of a traditional DSSS receiver, research in a noncoherent spread spectrum (SS) scheme called transmit reference (TR) has gained considerable interest in recent times. In this noncoherent approach, the transmitter sends the unmodulated spreading signal as a *reference* along with the modulated *information* signal, separated by a small time offset [1]. The receiver despreads the information by correlating the received signal with itself, after realigning in time by the known time offset.

Although the concept dates back to 1950s [2], the TR scheme has gained renewed interest in the context of ultra-wideband (UWB) [3]. In a conventional time offset TR (ToTR) UWB system, the time offset is kept larger than the delay spread of the channel. A drawback of ToTR stems from the difficult implementation of the time offset, due to the challenging integration of the associated wideband delay element on a small chip [4]. To avoid the architectural complexity of ToTR, the separation of the reference and the information signals can be carried out through code multiplexing [5], frequency shift, or any other separating waveform [6], as summarized in [7]. The use of frequency offset was introduced in [8], where the authors presented a frequency offset TR (FoTR) system, also known as the frequency-shift reference (FSR) system; an idea that was independently proposed by Goeckel in [9], [10]. The frequency offsets are chosen such that the reference and the information signals are orthogonal over a symbol duration [9]. Adhering to this guideline, different frequency offsets can be used for different communication links to enable MA in the network [11]. In [10], [12], FoTR-UWB technique was studied in a multipath fading environment using standard IEEE UWB channel models. In [10], the bit-error-rate (BER) expression was derived, conditioned on a channel

Manuscript received March 25, 2019; revised July 23, 2019 and October 12, 2019; accepted October 16, 2019. Date of publication November 4, 2019; date of current version February 11, 2020. This work was supported by the Netherlands Organization for Scientific Research (NWO) under its domain Applied and Technical Sciences (TTW) through the Project WALNUT under Grant 11317. The associate editor coordinating the review of this article and approving it for publication was R. Dinis. *(Corresponding author: Ibrahim Bilal.)*

I. Bilal was with the Telecommunication Engineering Group, University of Twente, 7500 AE Enschede, The Netherlands. He is now with Xsens B.V., 7500 AN Enschede, The Netherlands (e-mail: i.bilal@utwente.nl).

A. Meijerink was with the Telecommunication Engineering Group, University of Twente, 7500 AE Enschede, The Netherlands. He is now with LioniX International BV, 7500 AL Enschede, The Netherlands (e-mail: a.meijerink@ieee.org).

M. J. Bentum was with the Telecommunication Engineering Group, University of Twente, 7500 AE Enschede, The Netherlands. He is now with the Electromagnetics Group, Eindhoven University of Technology, 5600 MB Eindhoven, The Netherlands (e-mail: m.j.bentum@tue.nl).

Color versions of one or more of the figures in this article are available online at http://ieeexplore.ieee.org.

Digital Object Identifier 10.1109/TWC.2019.2949783

realization. The performance was shown to be in par with that of a ToTR-UWB system.

The FoTR system imposes few restrictions on the choice of the frequency offset. A large frequency offset (compared to the channel coherence bandwidth) can lead to decoherence between the reference and the information signal, resulting in a poor signal-to-noise ratio (SNR). The performance degradation due to this *reference decoherence* (RD) was partially considered in [6], [10]. However, it needs a more thorough investigation. In an MA network, where a number of concurrent links needs to be established, large values of frequency offsets are essential. Thus, the limitation on the maximum usable value of the frequency offset jeopardizes the scalability of the FoTR networks. Moreover, since the choice of the frequency offset is tied to the symbol duration, the constraints on the frequency offset can also limit the maximum data rate. Besides a limited research on the implications of the choice of the design parameters, the studies so far have focused on the average BER of the FoTR system, which is a useful metric when there are fast changes in the radio environment. In monitoring applications, where the channel can be considered more or less static over one burst of transmission, the outage probability is a more meaningful metric than the average BER.

The *self-correlation* operation of the TR receiver enhances the overall noise. A drawback of the UWB TR system is the pronounced impact of noise, whose power scales with the operational bandwidth. Moreover, the widely-applied channel models are also somewhat restrictive, primarily because they involve a lot of parameters, which fail to provide an intuitive understanding of the interplay between the propagation environment and performance. Besides, there have also been a few reservations about the interpretation of these channel models [13]. In order to assess the feasibility of the FoTR system for monitoring applications in NLOS environments, we need a framework for determining suitable performance metrics, given system and channel parameters, so that we can find reasonable system parameters that optimize the performance.

This article takes a wideband approach to FoTR, with bandwidths in the order of tens of megahertz, as a candidate for operation in the unlicensed bands (such as 2.4 or 5 GHz ISM band). Compared to the UWB system, the wideband system offers lower instantaneous data rates, but has a reduced power demand. A proof-of-concept receiver for such a system was developed, with an instantaneous power consumption of less than $200\,\mu$W [14]. From an analytic perspective, a wideband channel model helps describe the performance in terms of a single channel parameter. In our previous study [15], we investigated a wideband FoTR system using a noise-based carrier in a dense multipath fading environment, assuming a brick-wall spectrum of the spreading signal. Average BER was derived and studied. The results indicated that, although an increase in the spreading factor improves the performance in the high-SNR regime, the collective noise in the receiver is enhanced by an increase in the transmission power.

This article extends that analysis, beginning with a generalization of the system model. The novel contribution of this study is twofold. First, we investigate the interplay between delay dispersion and the choice of the frequency offset, and formulate a rule-of-thumb criterion for the maximum usable frequency offset. Second, we derive and analyze the outage probability of the FoTR system. An exact closed-form expression for the outage probability, although much desired, may not be realizable. Applying a few approximations on the SNR parameters enables us to derive a closed-form expression for the outage probability.

The article is structured as follows. The communication model is outlined in Sec. II. This is followed by Sec. III, where we derive the SNR and BER, conditioned on a channel realization. We further quantify the distortions due to inter-symbol-interference (ISI) and RD, brought about by the delay-dispersiveness of the channel. Building on the results, we derive an approximated closed-form expression for the outage probability. Numerical examples and simulation results are discussed in Sec. IV, followed by a summary of key findings in Sec. V.

II. System Model

In this section, we present the FoTR communication model. For mathematical convenience, all bandpass signals will be represented in their complex baseband equivalent forms. A complex envelope of any bandpass signal $s(t)$ will be denoted by $\tilde{s}(t)$. Properties of complex baseband signals and systems [16] will be frequently applied.

A. Transmitter Model

We consider a binary FoTR communication system[1] as shown in Fig. 1, where the insets depict power spectral densities[2] (PSDs) of the corresponding signals. The transmitter generates a spreading signal, modeled as a wide-sense-stationary (WSS) Gaussian bandpass process centered around a radio frequency[3] (RF) f_{c}. The complex envelope $\tilde{x}(t)$ of $x(t)$ has a two-sided PSD

$$S_{\tilde{x}}(f) = \frac{2P_x}{B_x}\,\mathcal{S}\left(\frac{f}{B_x}\right), \tag{1}$$

where P_x is the mean power in the bandpass signal $x(t)$; B_x is the bandwidth; $\mathcal{S}(\nu)$ is the normalized shape of the PSD with unit width and unit area; and ν is the normalized frequency. In our previous work, we studied the implications of the spectral shape $\mathcal{S}(\nu)$ on performance [17]. For consistency with the analysis in that study, the spectral shape is defined such that

$$\int_{-\infty}^{\infty} \mathcal{S}^2(\nu)\,\mathrm{d}\nu = \int_{-\infty}^{\infty} \mathcal{S}(\nu)\,\mathrm{d}\nu = 1. \tag{2}$$

In this article, we will apply (and clearly mention) a few important conclusions from that study. For a detailed analysis of an optimal spectral shape $\mathcal{S}(\nu)$, interested readers are directed to [17]. The spreading signal spreads a message signal

[1]The transmitter architecture is unchanged w.r.t. our previous work [17].

[2]The FoTR and the FSR-UWB differ primarily in their bandwidths and the nature of their spreading signals.

[3]The center frequency and bandwidth are assumed such that the US assumption (discussed in Sec. II-B) can be applied.

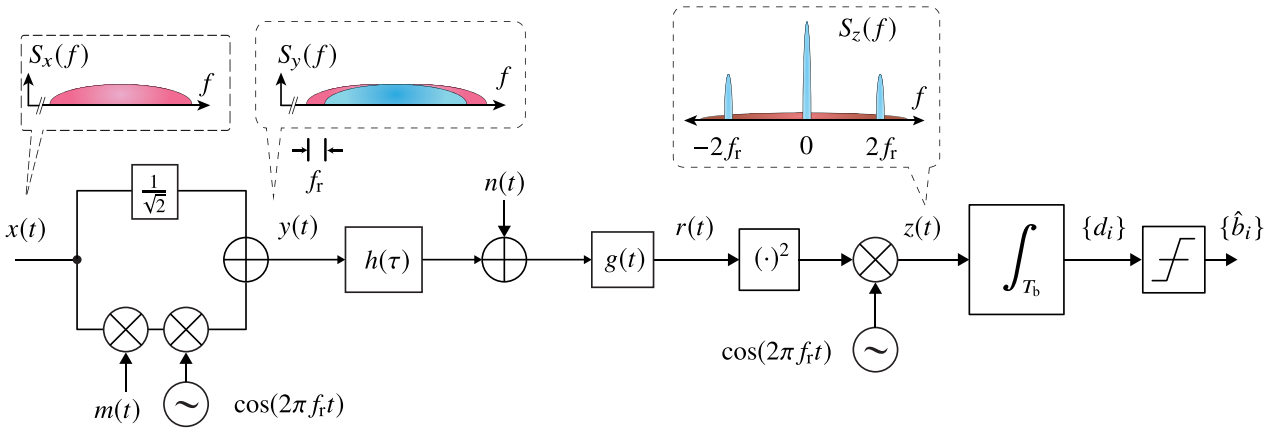

Fig. 1. A binary FoTR communication model, with insets depicting power spectral densities (PSDs).

$m(t)$ at one branch of the transmitter. On the other branch, the spreading signal is sent as a reference signal. The message signal is chosen to be a binary bipolar non-return-to-zero (NRZ) signal[4] with a rectangular pulse shape, i.e.,

$$m(t) = \sum_{i=-\infty}^{\infty} b_i p\left(t - i\,T_\mathrm{b}\right), \tag{3}$$

where $p(t)$ is a unit-amplitude rectangular pulse of duration T_b; i is the data index; and b_i is a binary information bit, taking values ± 1 with equal probability. A frequency offset $f_\mathrm{r} \ll B_x$, already known to the receiver, is applied to the information signal. As a design parameter, f_r is chosen to be an integer multiple of the symbol rate, i.e., $f_\mathrm{r} = c/T_\mathrm{b}$ for a positive integer c. Such a choice establishes orthogonality between the reference and the information signal over one symbol time. This will be discussed in the next section. For the current model, we assume f_r to be much smaller than the coherence bandwidth B_c of the channel. The implications of using large values for the frequency offsets (leading to RD) will be addressed in Sec. III-B.

The transmitter linearly combines the information and the reference signal. The FoTR signal $y(t)$, sent over the wireless channel, has a complex envelope

$$\tilde{y}(t) = \tilde{x}(t)\Big[1/\sqrt{2} + m(t)\cos(2\pi f_\mathrm{r} t)\Big] = \tilde{x}(t)a(t), \tag{4}$$

where we have defined the narrowband term

$$a(t) = 1/\sqrt{2} + m(t)\cos(2\pi f_\mathrm{r} t), \tag{5}$$

and the factor $1/\sqrt{2}$ is applied to ensure equal power distribution between the reference and the information signals. The PSD of the FoTR signal is depicted in the second inset in Fig. 1. Since we have chosen $f_\mathrm{r} \ll B_x$, the bandwidth of the FoTR signal $y(t)$ is approximately B_x.

B. Channel Model

We consider a dense multipath channel which is assumed linear and time-invariant (LTI) over one burst of transmission. The channel impulse response, denoted by $h(\tau)$, is assumed to be a Gaussian process [18], with a complex envelope $\tilde{h}(\tau)$ and the complex baseband transfer function $\widetilde{H}(f)$. To distinguish between delay dispersion and absolute time, τ will be used for the delays, and t for the absolute time. The channel is considered to obey the uncorrelated scatterers (US) assumption. This implies that the autocorrelation function (ACF) of the impulse response is

$$R_{\tilde{h}}(\tau, \tau') = \mathbb{E}_h\big[\tilde{h}(\tau)\tilde{h}^*(\tau')\big] = P_h(\tau)\,\delta(\tau - \tau'), \tag{6}$$

where $\mathbb{E}_h[\,\cdot\,]$ denotes expectation over the channel ensemble, and $P_h(\tau)$ is the power delay profile (PDP) of the channel. Denoting L as the average propagation loss, the average channel gain is

$$\mathbb{E}_h\big[|H(f)|^2\big] = \frac{1}{4}\mathbb{E}_h\big[|\widetilde{H}(f)|^2\big] = \frac{1}{4}\int_0^\infty P_h(\tau)\,\mathrm{d}\tau = \frac{1}{L}. \tag{7}$$

The channel has a certain rms delay spread τ_rms and a maximum excess delay τ_m. The analysis in this article assumes $\tau_\mathrm{rms} \gg 1/B_x$ to model a frequency-selective multipath channel. Since we operate at very low data rates, we assume that the symbol time is much larger than the delay spread, i.e., $\tau_\mathrm{rms} \ll T_\mathrm{b}$. This assumption guarantees a scenario free from ISI. This is only valid for a particular environment. For a much larger delay spread, the impairments due to delay dispersion cannot be ignored. This will be addressed later in Sec. III-B.

C. Receiver Model

The transmitted signal $y(t)$ is perturbed by the channel, and additive noise $n(t)$ which is modeled as a zero mean WSS Gaussian process with spectral density $N_0/2$. At the output of the receiver front-end (RFE) filter with impulse response $g(t)$, we obtain

$$r(t) = h(t) \otimes g(t) \otimes y(t) + g(t) \otimes n(t), \tag{8}$$

where $\otimes$ denotes convolution. The design choices $\tau_\mathrm{rms} \ll T_\mathrm{b}$ and $f_\mathrm{r} = c/T_\mathrm{b} \ll B_\mathrm{c}$ enable the system to operate unimpaired by ISI and RD. Hence, we can ignore the variations in the narrowband term $a(t)$ in (5) over the duration of $h(\tau)$.

[4]For simplicity, we have considered binary phase shift keying (BPSK). This can be easily extended to higher order modulation techniques, given that the frequency offsets are chosen in accordance with the symbol duration.

Similarly, for $1/T_{\rm b} \ll B_x$, we can ignore the effect of $g(t)$ on $a(t)$. For notational convenience, we denote the wideband signals filtered by the front-end filter as

$$x_g(t) = g(t) \otimes x(t) \Rightarrow \tilde{x}_g(t) = \frac{1}{2}\tilde{g}(t) \otimes \tilde{x}(t) \tag{9a}$$

$$n_g(t) = g(t) \otimes n(t) \Rightarrow \tilde{n}_g(t) = \frac{1}{2}\tilde{g}(t) \otimes \tilde{n}(t) \tag{9b}$$

Note that $\{x_g(t), n_g(t)\}$ are zero-mean WSS processes. Applying the above-mentioned assumptions and notations, the received signal in (8) can be rewritten as

$$r(t) = \big(h(t) \otimes x_g(t)\big)a(t) + n_g(t). \tag{10}$$

We now remark on the RFE filter and use important conclusions from our study on spectral shapes and transfer function of the RFE filter [17]. We had found that for a noise-based FoTR link in a frequency-flat channel, an optimal[5] RFE filter exists which maximizes the SNR of the decision variable. However, the transfer function of the optimal filter needs to be adapted to the received signal and noise levels, making it practically infeasible in most cases. We also presented a practical albeit suboptimal filter. The transfer function of the suboptimal filter is matched to the spectral shape of the spreading signal, i.e.,

$$|G(f)|^2 = \mathcal{S}\left(\frac{f-f_{\rm c}}{B_x}\right) + \mathcal{S}\left(\frac{f+f_{\rm c}}{B_x}\right) \Rightarrow |\widetilde{G}(f)|^2 = 4\mathcal{S}\left(\frac{f}{B_x}\right). \tag{11}$$

It was shown that such a filter is close to optimal for low carrier-to-noise ratios (CNRs). For higher CNRs, it is close to optimal if the spreading signal has a uniform PSD and a sharp roll off, such as the Butterworth shape of a high order. For such a spectral shape, it is evident that the suboptimal filter will effectively capture the desired signal and suppress all out-of-band signals.

In this article, we will consider $g(t)$ to be the impulse response of the suboptimal filter. Subsequently, the complex envelopes of the filtered signal and noise in (9) have PSDs

$$S_{\tilde{x}_g}(f) = \frac{1}{4}S_{\tilde{x}}(f)\left|\widetilde{G}(f)\right|^2 = \frac{2P_x}{B_x}\mathcal{S}^2\left(\frac{f}{B_x}\right), \tag{12a}$$

$$S_{\tilde{n}_g}(f) = \frac{1}{4}(2N_0)\left|\widetilde{G}(f)\right|^2 = 2N_0\,\mathcal{S}\left(\frac{f}{B_x}\right). \tag{12b}$$

The receiver restores the message bit by a self-correlation operation. The received signal is mixed with itself and then re-aligned in frequency using the known frequency offset $f_{\rm r}$. The local oscillator at the receiver is assumed perfectly locked in phase and frequency to that in the transmitter. Assuming perfect symbol-level synchronization, the input to the detection filter is

$$\begin{aligned} z(t) &= r^2(t)\cos(2\pi f_{\rm r}t) = \frac{1}{2}|\tilde{r}(t)|^2\cos(2\pi f_{\rm r}t) + \text{HFC} \\ &= z_{yy}(t) + z_{yn}(t) + z_{nn}(t) + \text{HFC}, \end{aligned} \tag{13}$$

where HFC denotes high-frequency components around $2f_{\rm c}$; and the signal self-mixing, the signal-noise mixing, and the noise self-mixing products are respectively defined as

$$z_{yy}(t) = \frac{1}{8}\left|\int_{-\infty}^{\infty}\tilde{h}(u)\tilde{x}_g(t-u)\,{\rm d}u\right|^2 a^2(t)\cos(2\pi f_{\rm r}t), \tag{14a}$$

$$\begin{aligned} z_{yn}(t) = \frac{1}{4}\int_{-\infty}^{\infty}\Big(\tilde{h}(u)\tilde{x}_g(t-u)\tilde{n}_g^*(t) + \tilde{h}^*(u)\tilde{x}_g^*(t-u)\tilde{n}_g(t)\Big){\rm d}u \\ \cdot\, a(t)\cos(2\pi f_{\rm r}t), \end{aligned} \tag{14b}$$

$$z_{nn}(t) = \frac{1}{2}\left|\tilde{n}_g(t)\right|^2\cos(2\pi f_{\rm r}t). \tag{14c}$$

Note that these cross-products add to the overall noise. The bandwidth of each mixing product, and hence that of $z(t)$ is in the order of B_x. The despread message signal lies in the signal self-mixing product $z_{yy}(t)$. The overall wideband noise and the narrowband despread signal are shown in the third inset of Fig. 1.

Since we have assumed a polar NRZ signaling scheme, we consider an integrate-and-dump filter (IDF) to recover the desired information. Note that the bandwidth of the IDF ($1/T_{\rm b}$) is much smaller than that of $z(t)$. In other words, the integration time is much larger than the correlation time of $z(t)$. We invoke the Central Limit Theorem (CLT), and approximate the sample d_i, at the output of the IDF, to be Gaussian distributed. Finally, since the IDF is a low-pass filter, the HFC will be suppressed, and, henceforth, ignored in the analysis.

Before proceeding further, we remark on the CLT approximation. The input to the IDF, given in (13), is a linear combination of χ^2 distributed random variables (RVs). The convergence of a sum of χ^2 distributed RVs to a Gaussian RV is slow [19], and a large number of samples is required for a high accuracy in the tails of the distribution. This implies that in our case, B_x has to be much larger than $1/T_{\rm b}$ for the approximation to hold. In other words, a small spreading factor $S = B_xT_{\rm b}$ leads to a weak CLT approximation. Therefore, the analysis and results in this article are more accurate for large values of S. This should not be a major concern in practice, since we consider low data rates and large bandwidths in order to benefit from the features of the SS system.

III. Performance Analysis

In this section, a detailed performance analysis of the noise-based FoTR link in dense multipath fading channels is provided. First, Sec. III-A provides a derivation of an expression for the conditional SNR and average BER. Next, an understanding of the impairments (RD and ISI) due to delay dispersion is presented in Sec. III-B; and finally, an approximated expression for the outage probability is derived in Sec. III-C. It must be stated that the derivation of the BER in Sec. III-A is not entirely a novel contribution. With a simplified system and channel model, the analysis was previously carried out in [15]; this will be discussed in Sec. III-C.

A. Signal-to-Noise Ratio

To derive an expression for the SNR, we need to derive the statistics of the decision variable d_i. Without loss of generality,

[5]This is similar to finding an optimum LTI filter for detection of a known signal in additive white Gaussian noise (AWGN).

we consider the data index $i=0$. The decision variable is

$$d_0 = \int_{-T_\mathrm{b}/2}^{T_\mathrm{b}/2} z(t)\,\mathrm{d}t = d_{yy} + d_{yn} + d_{nn}, \tag{15}$$

where the last equality follows from substituting $z(t)$ from (13), and denoting the contribution[6] from each mixing product to the decision variable as

$$d_{yy} = \int_{-T_\mathrm{b}/2}^{T_\mathrm{b}/2} z_{yy}(t)\,\mathrm{d}t, \tag{16a}$$

$$d_{yn} = \int_{-T_\mathrm{b}/2}^{T_\mathrm{b}/2} z_{yn}(t)\,\mathrm{d}t, \tag{16b}$$

$$d_{nn} = \int_{-T_\mathrm{b}/2}^{T_\mathrm{b}/2} z_{nn}(t)\,\mathrm{d}t. \tag{16c}$$

In the subsequent analysis, we derive the mean and variance of the decision variable. For brevity of notation, we drop the conditional variables $\{b_i, h\}$ in the subsequent analysis.

Mean of d_0: The mean of the decision variable follows from (15) and (16a) as

$$\mathbb{E}[d_0] = \mathbb{E}[d_{yy} + d_{yn} + d_{nn}] = \mathbb{E}[d_{yy}] + \mathbb{E}[d_{nn}], \tag{17}$$

where the last equality follows from evaluating (14b), recognizing that $n(t)$ and $x(t)$ are mutually independent zero-mean processes.

The mean contribution from the signal self-mixing product $z_{yy}(t)$ to the mean of d_0 follows from (14a), and (16a) as

$$\begin{aligned}\mathbb{E}[d_{yy}] &= \frac{1}{8}\int_{-T_\mathrm{b}/2}^{T_\mathrm{b}/2} a^2(t)\cos(2\pi f_\mathrm{r} t) \\ &\quad\cdot \int_{-\infty}^{\infty}\int_{-\infty}^{\infty} \tilde{h}(u)\tilde{h}^*(v)\,\mathbb{E}\big[\tilde{x}_g(t-u)\tilde{x}_g^*(t-v)\big]\,\mathrm{d}u\,\mathrm{d}v\,\mathrm{d}t \\ &= \frac{1}{8}\int_{-T_\mathrm{b}/2}^{T_\mathrm{b}/2} a^2(t)\cos(2\pi f_\mathrm{r} t)\,\mathrm{d}t \\ &\quad\cdot \int_{-\infty}^{\infty}\int_{-\infty}^{\infty} R_{\tilde{x}_g}(v-u)\tilde{h}(u)\tilde{h}^*(v)\,\mathrm{d}u\,\mathrm{d}v,\end{aligned}$$

where $R_{\tilde{x}_g}(\tau)$ is the ACF of $\tilde{x}_g(t)$. Substituting $a(t)$ from (5) and $m(t)$ from (3), we solve

$$\begin{aligned}\mathbb{E}[d_{yy}] &= \frac{1}{8}\int_{-\infty}^{\infty}\int_{-\infty}^{\infty} R_{\tilde{x}_g}(v-u)\tilde{h}(u)\tilde{h}^*(v)\,\mathrm{d}u\,\mathrm{d}v \\ &\quad\cdot \int_{-T_\mathrm{b}/2}^{T_\mathrm{b}/2}\cos(2\pi f_\mathrm{r} t) \\ &\quad\cdot \left(\frac{1}{2} + \sqrt{2}b_0\cos(2\pi f_\mathrm{r} t) + \cos^2(2\pi f_\mathrm{r} t)\right)\,\mathrm{d}t.\end{aligned} \tag{18}$$

The integrand in the integral over t is a summation of an information bearing term with other undesired bias terms. Using elementary calculus and trigonometry, it can be shown that the bias terms will be suppressed if $f_\mathrm{r} = c/T_\mathrm{b}$ for $c \in \mathbf{Z}^+$, resulting in

$$\mathbb{E}[d_{yy}] = \frac{b_0 T_\mathrm{b}}{8\sqrt{2}}\int_{-\infty}^{\infty}\int_{-\infty}^{\infty} R_{\tilde{x}_g}(v-u)\tilde{h}(u)\tilde{h}^*(v)\,\mathrm{d}u\,\mathrm{d}v. \tag{19}$$

[6]Since $x(t)$ is a noise process, d_{yy} in FoTR is not a deterministic term, in contrast to that in the TR-UWB systems.

This choice of the frequency offset ($f_\mathrm{r} = c/T_\mathrm{b}$) is an important design criterion for an FoTR system that employs an NRZ signaling scheme.[7]

The contribution from the noise self-mixing product $z_{nn}(t)$ to the mean of d_0 follows from (14c), and (16c) as

$$\begin{aligned}\mathbb{E}[d_{nn}] &= \frac{1}{2}\int_{-T_\mathrm{b}/2}^{T_\mathrm{b}/2} \mathbb{E}\Big[\big|\tilde{n}_g(t)\big|^2\Big]\cos(2\pi f_\mathrm{r} t)\,\mathrm{d}t \\ &= \frac{1}{2}R_{\tilde{n}_g}(0)\int_{-T_\mathrm{b}/2}^{T_\mathrm{b}/2}\cos(2\pi f_\mathrm{r} t)\,\mathrm{d}t = 0,\end{aligned}$$

where $R_{\tilde{n}_g}(\tau)$ represents the ACF of $\tilde{n}_g(t)$; and the last equality follows if $f_\mathrm{r} = c/T_\mathrm{b}$ for a positive integer c, as discussed above. Consequently, the mean of the decision variable is given by (19). Using the Wiener-Khinchin relations, we write

$$\begin{aligned}\mathbb{E}[d_0] = \mathbb{E}[d_{yy}] &= \frac{b_0 T_\mathrm{b}}{8\sqrt{2}}\int_{-\infty}^{\infty} S_{\tilde{x}_g}(f)|\widetilde{H}(f)|^2\,\mathrm{d}f \\ &= \frac{b_0 T_\mathrm{b}\alpha_h}{2\sqrt{2}L}\int_{-\infty}^{\infty} S_{\tilde{x}_g}(f)\,\mathrm{d}f,\end{aligned} \tag{20}$$

where we have defined a channel variable,

$$\begin{aligned}\alpha_h &= \frac{\int_{-\infty}^{\infty} S_{\tilde{x}_g}(f)|\widetilde{H}(f)|^2\,\mathrm{d}f}{\mathbb{E}_h\left[\int_{-\infty}^{\infty} S_{\tilde{x}_g}(f)|\widetilde{H}(f)|^2\,\mathrm{d}f\right]} = \frac{L\int_{-\infty}^{\infty} S_{\tilde{x}_g}(f)|\widetilde{H}(f)|^2\mathrm{d}f}{4\int_{-\infty}^{\infty} S_{\tilde{x}_g}(f)\,\mathrm{d}f} \\ &= \frac{L}{4}\int_{-\infty}^{\infty}\mathcal{S}^2(\nu)\,|\widetilde{H}(\nu B_x)|^2\,\mathrm{d}\nu.\end{aligned} \tag{21}$$

In the above relation, the second equality follows from (7), and the last equality follows from (12a) and using the definition in (2). Note that $\mathbb{E}_h[\alpha_h] = 1$. Substituting the expression of $S_{\tilde{x}_g}(f)$ from (12a) in (20), and subsequently solving the integral, the mean of d_0 reduces to

$$\mathbb{E}[d_0] = \frac{b_0 P_x T_\mathrm{b}\alpha_h}{\sqrt{2}L}\int_{-\infty}^{\infty}\mathcal{S}^2(\nu)\,\mathrm{d}\nu = \frac{b_0 P_x T_\mathrm{b}\alpha_h}{\sqrt{2}L}, \tag{22}$$

where the last equality follows from (2). The above expression represents the mean of the decision variable, conditioned on the channel realization $h(\tau)$ and the bit b_0.

Variance of d_0: The variance of the decision variable, conditioned on the channel realization and the data sequence, can be written as

$$\sigma_{d_i}^2 = \int_{-T_\mathrm{b}/2}^{T_\mathrm{b}/2}\int_{-T_\mathrm{b}/2}^{T_\mathrm{b}/2} C_{zz}(t_1, t_2)\,\mathrm{d}t_1\,\mathrm{d}t_2, \tag{23}$$

where $C_{zz}(t_1, t_2)$ is the autocovariance function of $z(t)$. Since the processes $x(t)$ and $n(t)$ are mutually independent and have zero means, it can be shown that all mixing products in (14) are mutually uncorrelated. Therefore, the function $C_{zz}(t_1, t_2)$ can be written as the sum of the autocovariance functions of the individual mixing products. Denoting the contribution from any mixing product $z_{qs}(t)$ as Ψ_{qs}, (23) is written as

$$\sigma_{d_i}^2 = \Psi_{yy} + \Psi_{yn} + \Psi_{nn}. \tag{24}$$

[7]For a general signaling scheme with nonrectangular pulses, where the IDF is replaced by a matched filter, a sufficient condition $f_\mathrm{r} \gg 1/T_\mathrm{b}$ will enforce the orthogonality, and hence suppress the bias terms.

The noise contributions $\{\Psi_{yy}, \Psi_{yn}, \Psi_{nn}\}$ are derived in the appendix, and are given as

$$\Psi_{yy} = 25\beta_h P_x^2 T_\mathrm{b}\lambda_2/(16L^2 B_x), \tag{25a}$$
$$\Psi_{yn} = 5\vartheta_h P_x T_\mathrm{b} N_0 \lambda_1/(4L), \tag{25b}$$
$$\Psi_{nn} = N_0^2 B_x T_\mathrm{b}/2. \tag{25c}$$

In the above expressions, we have used a few undefined parameters. The parameters

$$\lambda_1 = \int_{-\infty}^{\infty} \mathcal{S}^3(\nu)\,\mathrm{d}\nu, \quad \lambda_2 = \int_{-\infty}^{\infty} \mathcal{S}^4(\nu)\,\mathrm{d}\nu, \tag{26}$$

quantify the dependence on the spectral shape $\mathcal{S}(\nu)$, and have nominal values $\{\lambda_1, \lambda_2\} \geq 1$ [17]. The channel parameters $\{\vartheta_h, \beta_h\}$, defined analogous to α_h in (21), are

$$\vartheta_h = \frac{\int_{-\infty}^{\infty} S_{\tilde{x}_g}(f)|\widetilde{H}(f)|^2|\widetilde{G}(f)|^2\,\mathrm{d}f}{\mathbb{E}_h\Big[\int_{-\infty}^{\infty} S_{\tilde{x}_g}(f)|\widetilde{H}(f)|^2|\widetilde{G}(f)|^2\,\mathrm{d}f\Big]} = \frac{L}{4\lambda_1}\int_{-\infty}^{\infty} \mathcal{S}^3(\nu)\,|\widetilde{H}(\nu B_x)|^2\,\mathrm{d}\nu, \tag{27a}$$

$$\beta_h = \frac{2\int_{-\infty}^{\infty} S^2_{\tilde{x}_g}(f)|\widetilde{H}(f)|^4\,\mathrm{d}f}{\mathbb{E}_h\Big[\int_{-\infty}^{\infty} S^2_{\tilde{x}_g}(f)|\widetilde{H}(f)|^4\,\mathrm{d}f\Big]} = \frac{L^2}{16\lambda_2}\int_{-\infty}^{\infty} \mathcal{S}^4(\nu)\,|\widetilde{H}(\nu B_x)|^4\,\mathrm{d}\nu, \tag{27b}$$

where (27a) follows from (7), (11) and (26); and (27b) follows from (26), and recognizing that the Gaussian assumption of the channel leads to

$$\mathbb{E}_h\Big[\big|\widetilde{H}(f)\big|^4\Big] = 2\,\mathbb{E}_h^2\Big[\big|\widetilde{H}(f)\big|^2\Big] = 32/L^2.$$

Having found the mean and variance of the decision sample, we can now derive the SNR. Substituting (25) in (24), in conjunction with (22), the SNR of d_0 is

$$\mathrm{SNR}(h) = \frac{\mathbb{E}^2[d_0|b_0, h]}{\sigma^2_{d_0}} = \frac{8\alpha_h^2\gamma^2}{25\lambda_2\beta_h\gamma^2/S + 20\lambda_1\vartheta_h\gamma + 8S}, \tag{28}$$

where $S = B_x T_\mathrm{b}$ is the spreading factor; $\gamma = E_\mathrm{b}/N_0$ is the received SNR per bit; and the average received bit energy is

$$E_\mathrm{b} = \int_{-T_\mathrm{b}/2}^{T_\mathrm{b}/2} \mathbb{E}\Big[\big(y(t)\otimes h(t)\big)^2\Big]\,\mathrm{d}t = \int_{-T_\mathrm{b}/2}^{T_\mathrm{b}/2} \mathbb{E}\big[a^2(t)\big]\,\mathbb{E}\Big[\big(x(t)\otimes h(t)\big)^2\Big]\,\mathrm{d}t = T_\mathrm{b}\int_{-\infty}^{\infty} S_x(f)\,\mathbb{E}_h\big[|H(f)|^2\big]\,\mathrm{d}f = \frac{1}{L}P_x T_\mathrm{b}. \tag{29}$$

The equation in (28) represents the conditional output SNR of a noise-based FoTR link in a dense frequency-selective fading channel. Since we have chosen the system parameters such that ISI and RD are negligible, the derived SNR expression mainly models the effect of fading and noise from self-mixing. We will remark on the other effects in Sec. III-B. From (28), we note that the SNR of FoTR suffers from self-interference ($\Psi_{yy} \neq 0$), in contrast to that of the FSR-UWB system [10, eq. (16)]. It implies that FoTR has a comparatively worse performance for high values of γ/S.

As the decision variable (d_0) is Gaussian distributed, the BER for the binary FoTR communication system, with equi-probable transmitted bits, is given by

$$\mathrm{BER}(h) = \mathrm{Q}\left(\sqrt{\mathrm{SNR}(h)}\right), \tag{30}$$

where $\mathrm{Q}(\cdot)$ is the Gaussian tail probability. The average link quality is given by

$$\overline{\mathrm{BER}} = \mathbb{E}_h\Big[\mathrm{BER}(h)\Big]. \tag{31}$$

A closed-form expression for the average BER is much desired, but that requires knowledge of the probability density function (pdf) of the SNR. This is complicated to derive since different channel parameters appear in the numerator and the denominator of $\mathrm{SNR}(h)$.

The performance of the FoTR NLOS link will vary with the channel state. Since the average BER is dominated by low values of $\mathrm{SNR}(h)$, the variations in $\mathrm{SNR}(h)$ can have a considerable impact on the average BER. If $B_x\tau_\mathrm{rms} \gg 1$, then the channel parameters $\{\alpha_h, \beta_h, \vartheta_h\}$ tend to approach their mean values $\{1, 2, 1\}$. The channel is said to be *hardened*, i.e., it behaves deterministically, and the SNR expression (28) for each channel realization approaches

$$\lim_{B_x\tau_\mathrm{rms}\to\infty} \mathrm{SNR}(h) = \mathrm{SNR} = \frac{8\gamma^2}{50\lambda_2\gamma^2/S + 20\lambda_1\gamma + 8S}. \tag{32}$$

The hardened channel case is a hypothetical scenario, in which the variations in $\mathrm{SNR}(h)$ are negligible. Therefore, this scenario provides a lower bound on the average BER. Ideally, one would choose the design parameters such that the overall performance approaches the bound.

B. Effects of Delay-Dispersion

In the last subsection, we ignored the effects of delay-dispersion by modeling $f_\mathrm{r}\tau_\mathrm{rms} \ll 1$, and hence, $\tau_\mathrm{rms}/T_\mathrm{b} \ll 1$. We define $\varphi = \tau_\mathrm{rms}/T_\mathrm{b}$ and $\varpi = f_\mathrm{r}\tau_\mathrm{rms}$ as indicators of ISI and RD respectively. Unlike in the previous subsection, we incorporate the effect of the channel on $a(t)$ in (8). Incorporating the change, the signal self-mixing product $z_{yy}(t)$ in (13) is rewritten as

$$z_{yy}(t) = \frac{1}{8}\Big|\int_{-\infty}^{\infty} \tilde{h}(u)\tilde{x}_g(t-u)a(t-u)\,\mathrm{d}u\Big|^2 \cos(2\pi f_\mathrm{r} t).$$

To analyze ISI and RD, we need to look at the effect of delay dispersion on the mean of the decision variable d_0, which, analogous to the analysis in Sec. III-A, is solved to

$$\mathbb{E}[d_0] = \mathbb{E}[d_{yy}] = \frac{1}{8}\int_{-T_\mathrm{b}/2}^{T_\mathrm{b}/2}\int_{-\infty}^{\infty}\int_{-\infty}^{\infty} \tilde{h}(u)\tilde{h}^*(v)R_{\tilde{x}_g}(v-u) \cdot a(t-u)a(t-v)\cos(2\pi f_\mathrm{r} t)\,\mathrm{d}u\,\mathrm{d}v\,\mathrm{d}t \approx \frac{1}{8}\int_{-\infty}^{\infty}\int_{-\infty}^{\infty} \tilde{h}(u)\tilde{h}^*(v)R_{\tilde{x}_g}(v-u)\,\mathrm{d}v \cdot \int_{-T_\mathrm{b}/2}^{T_\mathrm{b}/2} a^2(t-u)\,\mathrm{d}u\,\cos(2\pi f_\mathrm{r} t)\,\mathrm{d}t,$$

where the approximation follows from observing that the support of $R_{\tilde{x}_g}(v-u)$ is very narrow ($\sim 1/B_x$), and the function

$a(t)$ hardly varies over a time duration that corresponds to the width of the ACF. Substituting $a(t)$ from (5), the above expression is solved to

$$\mathbb{E}[d_0] = \frac{1}{8\sqrt{2}} \int_{-\infty}^{\infty} \int_{-\infty}^{\infty} \tilde{h}(u)\tilde{h}^*(v) R_{\tilde{x}_g}(v-u)\,\mathrm{d}v \cdot \cos(2\pi f_\mathrm{r} u) \int_{-T_\mathrm{b}/2}^{T_\mathrm{b}/2} m(t-u)\,\mathrm{d}u\,\mathrm{d}t + \Lambda,$$

where Λ, a by-product of the mixing operation, denotes a sum of undesired bias terms. The term is negligibly small if $2f_\mathrm{r}$ is much larger than the detection filter bandwidth $(1/T_\mathrm{b})$. Therefore, in practice, large values of the offsets should be chosen to minimize the bias.[8] Substituting $m(t)$ from (3) in the above expression, we get

$$\mathbb{E}[d_0] = \frac{1}{8\sqrt{2}} \int_{-\infty}^{\infty} \int_{-\infty}^{\infty} \tilde{h}(u)\tilde{h}^*(v) R_{\tilde{x}_g}(v-u)\,\mathrm{d}v \cdot \cos(2\pi f_\mathrm{r} u)\Big(b_0 R_p(u) + \sum_{i\neq 0} b_i R_p(iT_\mathrm{b}+u)\Big)\,\mathrm{d}u + \Lambda, \quad (33)$$

where $R_p(\tau)$ represents the ACF of $p(t)$, with $R_p(0) = T_\mathrm{b}$.

Comparing (33) with (19) for the ISI- and RD-free case, the delay dispersion can have two effects on the demodulated information signal. First, the received symbol is distorted due to ISI, indicated by the summation in (33). The longer the duration of the impulse response $\tilde{h}(u)$, the higher the number of interfering symbols.

Second, even for negligible ISI, i.e., when $\varphi = \tau_\mathrm{rms}/T_\mathrm{b} \ll 1$, the magnitude of the recovered sample is reduced, as signified by the term $\cos(2\pi f_\mathrm{r} u)$ in (33). The oscillator at the receiver is not locked in phase to the arriving MPCs. Therefore, the demodulated signal from each MPC suffers from a small phase offset; the detrimental effect is magnified for a large value of $\varpi = f_\mathrm{r}\tau_\mathrm{rms}$. In other words, the reference and information signals tend to be incoherent if one chooses a large f_r.

For further explanation, we consider negligible ISI, which can be ensured by duty-cycling or by choosing a low data rate. To find a bound on the performance reduction due to RD, we ignore Λ, and look at the hardened channel case. The latter assumption implies that the channel state attains its mean value at every time. Taking the average of (33) over the channel ensemble, we get

$$\mathbb{E}_h\Big[\mathbb{E}[d_0]\Big] = \frac{b_0 T_\mathrm{b}}{8\sqrt{2}} \int_{-\infty}^{\infty}\int_{-\infty}^{\infty} \mathbb{E}_h\big[\tilde{h}(u)\tilde{h}^*(v)\big] R_{\tilde{x}_g}(v-u) \cdot \cos(2\pi f_\mathrm{r} u)\,\mathrm{d}u\,\mathrm{d}v = \frac{b_0 T_\mathrm{b}}{8\sqrt{2}} R_{\tilde{x}_g}(0) \int_{-\infty}^{\infty} P_h(u)\cos(2\pi f_\mathrm{r} u)\,\mathrm{d}u = \frac{1}{4\sqrt{2}} b_0 P_x T_\mathrm{b}\,\mathrm{Re}\Big\{R_{\widetilde{H}}(f_\mathrm{r})\Big\}, \quad (34)$$

where the second equality follows from (6); and $R_{\widetilde{H}}(\Delta f)$ is the frequency correlation function of the channel, with $R_{\widetilde{H}}(0) = 4/L$. Fig. 2 depicts the normalized magnitude of $R_{\widetilde{H}}(\Delta f)$ for a channel with an exponential PDP, i.e.,

$$P_h(\tau) = \frac{4}{L\tau_\mathrm{rms}} \exp(-\tau/\tau_\mathrm{rms}), \quad \tau \geq 0. \quad (35)$$

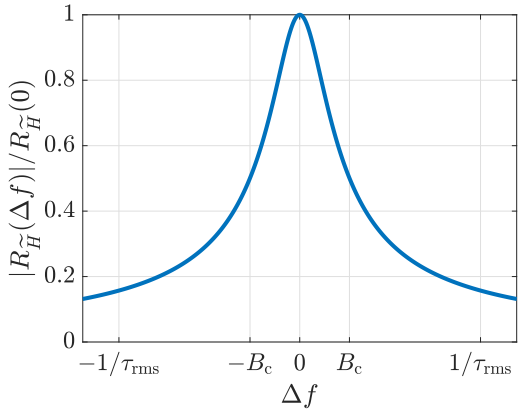

Fig. 2. Normalized frequency correlation function of an LTI channel with an exponential PDP, as a function of the frequency difference.

In the figure, B_c is depicted as the 3-dB bandwidth of the correlation function, which can be shown to be $\sqrt{3}/(2\pi\tau_\mathrm{rms})$. One can directly compare (34) to (22). An increase in the value of $f_\mathrm{r}/B_\mathrm{c}$ deteriorates the SNR performance. In other words, a large value of ϖ gives rise to RD. For an exponential PDP, one can solve that for a value $\varpi = \sqrt{3}/2\pi \approx 0.27$, one risks losing 75% of the recovered signal power. Small values of ϖ will have a smaller impact on the recovered energy. Nevertheless, RD will always have an influence.

Recall that the smallest recommended value of f_r is $1/T_\mathrm{b}$. Therefore, a large φ also leads to large ϖ; in other words, ISI is coupled with RD. If ISI is experienced in a link, RD will also be observed. The phenomenon will be explained with the help of figures in Sec. IV, with the aim to find a criterion on the highest usable frequency offset.

C. Outage Probability

In this section, we derive the outage probability of the FoTR system in dense fading channels. It is defined as the probability that the BER is worse than a certain *threshold* $\mathcal{E}_\mathrm{T}$, i.e.,

$$\mathbb{P}_\mathrm{out} = \Pr\left[\mathrm{BER}(h) \geq \mathcal{E}_\mathrm{T}\right] = \Pr\left[\mathrm{SNR}(h) \leq \Gamma_\mathrm{T}\right], \quad (36)$$

where we have defined an SNR threshold as $\Gamma_\mathrm{T} = [\mathrm{Q}^{-1}(\mathcal{E}_\mathrm{T})]^2$, which follows from (30).

To derive an exact expression for $\mathbb{P}_\mathrm{out}$, one needs to derive the joint-statistics of $\{\alpha_h, \beta_h, \vartheta_h\}$ in (28). However, since β_h is a complicated function of the random process $\widetilde{H}(f)$, the ensuing analysis is not straightforward, and may not necessarily lead to a closed-form expression. Allowing some approximations, we can derive a closed-form expression for the outage probability.

Approximations: First, we consider that the spectral shape $\mathcal{S}(\nu)$ is more or less uniform, such that $S_{\tilde{x}}(f)$ in (1) can be approximated as a brick-wall spectrum. One can verify that $\lambda_1 = \lambda_2 = 1$ in (26), and that $\vartheta_h = \alpha_h$ from (27a) and (21).

[8] Low values of f_r can also be problematic from implementation perspective, due to the high flicker noise.

Moreover, the channel can be accurately modeled using the well-known tapped-delay line (TDL) description, i.e.,

$$\tilde{h}(\tau) = \sum_k h_k \delta(\tau - k\Delta\tau), \tag{37}$$

where $\Delta\tau = 1/B_x$ is the resolvable delay bin; and $h_k \forall k$ are channel coefficients, modeled as circularly-symmetric complex Gaussian variables, i.e., $h_k \sim \mathcal{CN}(0, \sigma_k^2)$. Using the approximation and the TDL description of the channel, α_h and β_h in (21) and (27b) respectively solve to

$$\alpha_h = \frac{L}{4}\sum_k |h_k|^2, \quad \beta_h = \frac{L^2}{16}\sum_k \Big|\sum_l h_l h_{l-k}^*\Big|^2, \tag{38}$$

resulting in the SNR expression[9]

$$\mathrm{SNR}(h) = \frac{8\alpha_h^2\gamma^2}{25\beta_h\gamma^2/S + 20\alpha_h\gamma + 8S}. \tag{39}$$

Next, we remark on the relation between α_h and β_h. One can see from (38) that

$$\begin{aligned}\beta_h &= \alpha_h^2 + \frac{L^2}{16}\sum_{k\neq 0}\Big|\sum_l h_l h_{l-k}^*\Big|^2 \\ &= 2\alpha_h^2 + \frac{L^2}{16}\sum_{k\neq 0}\sum_l\sum_{m\neq l} h_l h_m^* h_{m-k} h_{l-k}^*. \end{aligned}\tag{40}$$

The parameter α_h is proportional to the gain in each channel realization. The second term in (40) represents the cross-energy of different channel taps. It can be seen from (40), that when α_h is low, β_h also tends to be low, and vice versa. The channel is considered to be in *deep fade* (i.e., $\mathrm{SNR}(h)$ in (39) is low) when α_h is low. Since an outage occurs when a deep fade occurs, we are only interested in low values of α_h. For such values, we approximate $\beta_h \approx 2\alpha_h^2$. We briefly postpone the discussion on the validity of the approximation, and apply it to see its utility. Using the approximations on the spectral shape $\mathcal{S}(\nu)$ and β_h, we can write (39) as

$$\mathrm{SNR}(h) \approx \widehat{\mathrm{SNR}}(h) = \frac{4\alpha_h^2\gamma^2}{25\alpha_h^2\gamma^2/S + 10\alpha_h\gamma + 4S}, \tag{41}$$

where $\widehat{\mathrm{SNR}}(h)$ denotes an approximated $\mathrm{SNR}(h)$. The SNR expression is now conditioned on a single channel parameter (α_h). Using the above expression in (36), we get

$$\mathbb{P}_{\mathrm{out}} \approx \Pr\left[\alpha_h^2\gamma^2(4 - 25\Gamma_{\mathrm{T}}/S) - 10\alpha_h\gamma\Gamma_{\mathrm{T}} - 4\Gamma_{\mathrm{T}}S \leq 0\right]. \tag{42}$$

With respect to the variable α_h, the argument of $\Pr[\,\cdot\,]$ in (42) is a quadratic inequality. Applying algebra, the positive solution of the inequality, denoted by α_{T}, is found to be

$$\alpha_{\mathrm{T}} = \frac{S}{\gamma}\cdot\frac{5 + 2\sqrt{(4S/\Gamma_{\mathrm{T}} - 25) + 25/4}}{4S/\Gamma_{\mathrm{T}} - 25}. \tag{43}$$

We refer to α_{T} as the threshold on the channel gain. The expression (42) can now be written as

$$\begin{aligned}\mathbb{P}_{\mathrm{out}} &= \Pr\left[\mathrm{SNR}(h) \leq \Gamma_{\mathrm{T}}\right] \approx \Pr\left[\widehat{\mathrm{SNR}}(h) \leq \Gamma_{\mathrm{T}}\right] \\ &= \Pr\left[\alpha_h \leq \alpha_{\mathrm{T}}\right]. \end{aligned}\tag{44}$$

[9]This simplified model with result (39) is a special case of (28), and was studied in our earlier work [15].

We now scrutinize the approximation $\beta_h \approx 2\alpha_h^2$. Using a simulation software, we generate a channel ensemble of 20,000 realizations for different values of $B_x\tau_{\mathrm{rms}}$. Since the approximations were used to simplify the expression of $\mathrm{SNR}(h)$, it is more meaningful to compare $\widehat{\mathrm{SNR}}(h)$ in (41) with $\mathrm{SNR}(h)$ in (39). We define the relative approximation error as

$$\epsilon_h = \left(\mathrm{SNR}(h) - \widehat{\mathrm{SNR}}(h)\right)/\mathrm{SNR}(h),$$

and plot it as a function of the channel variable α_h in Fig. 3. It is observed that the relative approximation error tends to be small, if α_h is small. Secondly, since the error ϵ_h leans towards a positive value, the approximated $\mathbb{P}_{\mathrm{out}}$ in (44) will tend to overestimate the outage probability for large values of α_h. Finally, the approximation is more accurate for low values of the CNR,[10] γ/S. For a fixed transmission power, a small CNR implies a large bandwidth B_x, which, as earlier discussed, tends to *harden* the channel. The SNR approaches a deterministic value and, hence, the approximation error tends to be negligible. To summarize, the approximations on $\mathcal{S}(\nu)$ and β_h are restrictive, and do not hold for all values of the system parameters. A large error can be expected for large values of γ/S. Nonetheless, $\beta_h = 2\alpha_h^2$ should hold fairly for small α_h; it will be later shown with simulation results that one can find the outage probability with a reasonable accuracy in cases of interest.

Probability distribution of α_h: In order to solve (44), one requires knowledge of the pdf of α_h. The parameter α_h in (38) is a sum of independent exponential distributed RVs, with each Gaussian element h_k having a zero mean but a distinct variance σ_k^2. The statistics of such an RV have been previously treated in renewal theory [20, p. 17] and more recently in the studies of MIMO systems [21]. It follows a generalized χ^2 distribution with a pdf

$$f_{\alpha_h}(u; K, \sigma_k^2) = \sum_{k=1}^{K}\frac{\exp(-u/\sigma_k^2)}{\sigma_k^2\prod_{j=1, j\neq k}^{K}\left(1 - \sigma_j^2/\sigma_k^2\right)}, \ \forall u \geq 0, \tag{45}$$

where K is the number of the exponential distributed RVs. In channel modeling, the impulse response (37) is usually truncated to a duration $K\Delta\tau$, such that most of the energy is received in that duration. In such case, K is a function of the maximum excess delay τ_m.

We define $C_{\mathrm{D}} = B_x\tau_{\mathrm{rms}}$ as the *channel diversity factor*, which roughly indicates the number of independent frequency bins in the channel transfer function. For two different values of C_{D}, we generate and plot the histograms of α_h in Fig. 4, along with a pdf estimate of α_h from (45). For reference, a pdf estimate of α_h using a Gaussian distribution is also plotted. We observe that owing to the CLT, the pdf of α_h approaches a Gaussian pdf for a very large C_{D}. Nonetheless, the Gaussian approximation poorly models the lower tail, and hence, will be inaccurate to estimate low values of $\mathbb{P}_{\mathrm{out}}$. On the other hand, the generalized χ^2 distribution accurately estimates the tail. Further simulations support this claim for different values of the channel diversity factor C_{D}.

[10]For our system, it can be shown that γ/S is in fact the CNR.

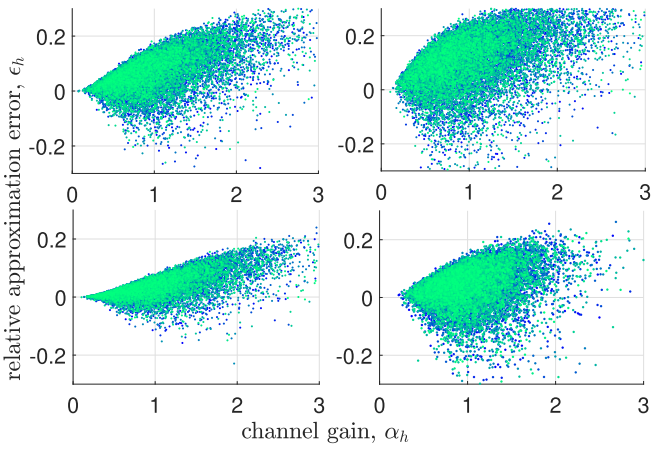

Fig. 3. Relative approximation error ϵ_h, plotted against α_h, for system parameters $\{B_x\tau_{\rm rms}, \gamma/S\}$ clockwise from top-left as $\{2, 0.5\}$, $\{2, 1\}$, $\{4, 0.5\}$, and $\{4, 0.25\}$.

Approximated outage probability: Using (45), the outage probability from (44) is rewritten as

$$\mathbb{P}_{\rm out} = \Pr\left[\alpha_h \le \alpha_{\rm T}\right] = \int_0^{\alpha_{\rm T}} f_{\alpha_h}(u, K, \sigma_k^2)\,{\rm d}u$$
$$= \sum_{k=1}^{K} \frac{1-\exp(-\alpha_{\rm T}/\sigma_k^2)}{\prod_{j=1, j\neq k}^{K}\left(1-\sigma_j^2/\sigma_k^2\right)}, \tag{46}$$

where $\alpha_{\rm T}$ is given in (43); and σ_k^2 follows from the PDP of the channel. The equation in (46) represents the approximated outage probability of an NLOS FoTR communication link.

In practice, a certain probability of outage is tolerated. In this case, the parameter of interest is the required $\gamma = E_{\rm b}/N_0$ at the receiver to remain below a tolerable level of the outage probability, ρ. We denote this parameter by γ_ρ. Using (46), γ_ρ is the positive and real root of the function

$$f(\gamma, \rho) = \sum_{k=1}^{K} \frac{1-\exp(-\alpha_{\rm T}/\sigma_k^2)}{\prod_{j=1, j\neq k}^{K}\left(1-\sigma_j^2/\sigma_k^2\right)} - \rho, \tag{47}$$

where γ is manifested in $\alpha_{\rm T}$. The equation does not seem to be analytically solvable. Therefore we will numerically evaluate the above function to find γ_ρ.

IV. Results and Discussion

In Sec. III, we derived an expression for the average BER; provided an understanding of the impairments due to delay dispersion; and derived an approximated closed-form-expression for the outage probability. A number of interrelated system and channel parameters influence the overall performance, often antagonistically. These parameters have key importance in design and implementation of an FoTR system. In this section, we investigate and discuss the performance of an NLOS FoTR link, subject to the different channel impairments. Furthermore, interplays between system parameters and propagation effects will be explored, in order to gain insights into the underlying mechanisms. We begin with a description of the simulation framework in Sec. IV-A. In Sec. IV-B, we study FoTR in a LOS AWGN channel, in order to outline the underlying mechanisms. Next, we study the performance trends in a multipath propagation environment. Since the environment can have multiple effects on the link's performance, we isolate and discuss these effects separately. We study the effect of fading in Sec. IV-C, followed by that of delay dispersion in Sec. IV-D. Finally, results on the outage probability of the FoTR link are presented in Sec. IV-E.

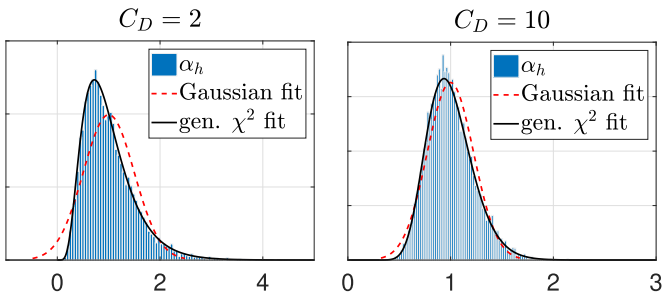

Fig. 4. Generalized χ^2 and Gaussian pdf fits onto the histograms of α_h for two different values of the channel diversity factor.

A. Simulation Framework

The channel model used in the simulation framework is based on the TDL channel description, and an exponential PDP (35) is considered.[11] The channel impulse response in (37) is truncated to a length $K = 5B_x\tau_{\rm rms}$; the duration corresponds to 99% of the total energy. The PSD of the noise-based spreading signal is shaped by a type-II Chebychev filter with a 40 dB stopband ripple, resulting in a uniform spectrum with a sharp roll-off.

For a particular multipath environment (fixed $\tau_{\rm rms}$), we generate a set of NLOS channel realizations, and simulate the FoTR system, sending blocks of information over each channel realization, obtaining a simulated BER(h) value. The $\overline{\rm BER}$ *simulation* results are found by averaging the BER over the ensemble. For the outage probability, the simulation results are obtained by finding the percentage of the total number of the channel realizations, over which the simulated link results in BER$(h) > \mathcal{E}_{\rm T}$. For a better estimate of $\mathbb{P}_{\rm out}$, the simulation is run multiple times to ensure that the percentage is computed upon at least 100 channel realizations in deep fade. Next, we find the *semi-analytical* results for $\overline{\rm BER}$, and theoretical results for $\mathbb{P}_{\rm out}$. The semi-analytical $\overline{\rm BER}$ is found by first computing $\{\alpha_h, \beta_h\}$ for a given channel, and then evaluating (39), (30), and (31). The theoretical results for $\mathbb{P}_{\rm out}$ are found by evaluating (46).

We will frequently interpret our results in terms of the composite parameters, $C_{\rm D} = B_x\tau_{\rm rms}$, $\varphi = \tau_{\rm rms}/T_{\rm b} = C_{\rm D}/S$, and $\varpi = f_{\rm r}\tau_{\rm rms}$. The individual parameters, such as the data rate $1/T_{\rm b}$, the bandwidth B_x, and the delay spread $\tau_{\rm rms}$ are kept in the ranges $[5, 15]$ kbps, $[10, 30]$ MHz, and $[50, 600]$ ns respectively. Moreover, unless specified otherwise, the frequency offset is chosen as a unit multiple of the symbol rate i.e., $f_{\rm r} = 1/T_{\rm b}$. Such a choice implies that $\varpi = \varphi$ for a given channel environment (fixed $\tau_{\rm rms}$).

[11] Nonetheless, the main analytical results (28) and (46) are applicable to all types of PDP.

B. Effect of Noise

To present the underlying mechanisms of FoTR, we first study the system's performance in a frequency-flat AWGN channel. The SNR expression for such a link can be found by substituting $\alpha_h = \vartheta_h = \beta_h = 1$ in (28). We simulate the LOS FoTR link, and plot the BER against increasing values of $\gamma = E_{\rm b}/N_0$ for different values of the spreading factor in Fig. 5. As a reference, we also plot the performance curve for FSR [10, eq. (10)], and that of BPSK in an AWGN channel.

We summarize the underlying mechanism; the details can be found in earlier studies [8], [22]. First, the FoTR link in a LOS scenario has a huge performance penalty. This is due to the mixing of all in-band signals at the receiver, which elevates the overall noise level. Particularly, the noise (with power Ψ_{yy}) from mixing of the desired signal with itself increases with increasing γ. This leads to the disagreements in performance with FSR, which does not model inter-pulse-interference (IPI). However, it must be stressed that for a given value of S, the FSR-UWB system offers much lower data rates, in comparison with the FoTR system.

We further observe that it is better to choose a low spreading factor in the low-SNR regime; this is because an increase in the spreading factor magnifies the noise contribution from AWGN. Furthermore, the performance benefits of using a large spreading factor are materialized only for high values of γ. Therefore, there exists an optimum value $S_{\rm opt}$ of the spreading factor for each value of γ, which maximizes the SNR for that particular value of γ. For the LOS AWGN link, one can show that $S_{\rm opt} = 5\gamma\sqrt{2\lambda_2}/4$, by finding the maximum of the SNR with respect to S.

Finally, we comment on the differences between the simulation and theoretical results. For small values of S, the theoretical curves diverge from the simulation, particularly at large values of γ. This is because the CLT is inaccurate in estimating the tail of the Guassian pdf. One needs very high numbers of samples (very large spreading factors) for accuracy at low values of BER. Nonetheless, the disparity is slight in the region of interest. For $S = 20$ dB, the difference in γ (between theory and simulation) to achieve a BER of 10^{-3} and 10^{-6} is 1 and 3 dB respectively, whereas for $S = 23$ dB it is 0.2 and 1 dB respectively.

C. Effect of Fading

We now discuss the effects of fading. We generate a channel ensemble of 1000 realizations, and simulate an FoTR communication system for two different values of the spreading factor. To isolate the effect of fading from delay dispersion, we choose the system parameters such that RD and ISI have a negligible impact, i.e., we have chosen $\varpi = \varphi \ll 1$. Fig. 6 and Fig. 7 illustrate the simulated and semi-analytical $\overline{\rm BER}$ for the FoTR link in a dense frequency-selective fading channel for different values of $C_{\rm D}$. As a reference, we also plot the performance curve for the FSR-UWB system [10, eq. (16)].

We observe that multipath fading deteriorates the overall link performance. A higher channel diversity factor improves the performance. However, the improvement is less compared to that experienced by the FSR-UWB system. As earlier mentioned, this is due to the self-interference (Ψ_{yy}), which has a much more significant impact at high values of $E_{\rm b}/N_0$.

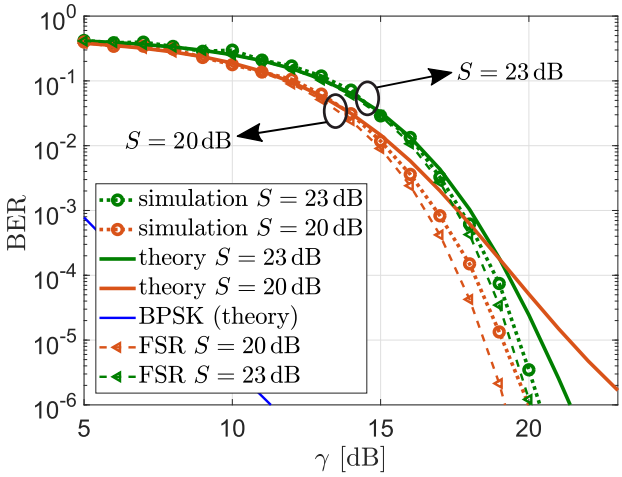

Fig. 5. BER against $\gamma = E_{\rm b}/N_0$ of the FoTR system in an AWGN channel.

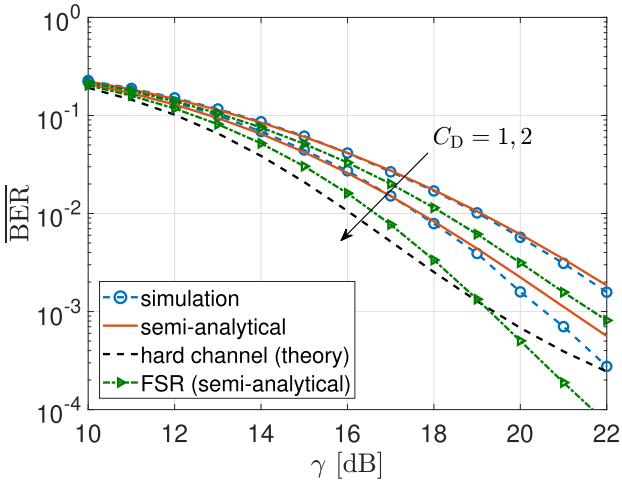

Fig. 6. $\overline{\rm BER}$ versus $\gamma = E_{\rm b}/N_0$ for different values of the channel diversity factor $C_{\rm D}$, and a fixed $S = 20$ dB, in a scenario with negligible ISI and RD.

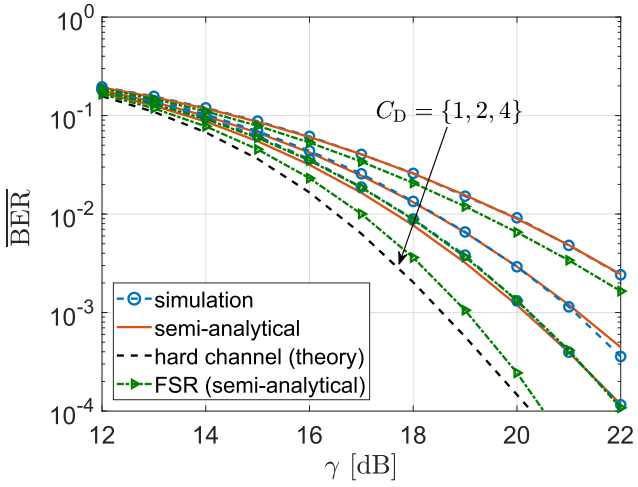

Fig. 7. $\overline{\rm BER}$ versus $\gamma = E_{\rm b}/N_0$ for different values of the channel diversity factor $C_{\rm D}$, and a fixed $S = 23$ dB, in a scenario with negligible ISI and RD.

Finally, as $C_{\mathrm{D}} \to \infty$, the channel is *hardened*, with the SNR expression given in (32). For this hypothetical scenario, a performance curve is depicted in the figure. The performance of the FoTR system approaches this curve (in theory) as C_{D} increases. However, this can also lead to an increase in φ or ϖ, which implies that the link will suffer performance deterioration due to RD or ISI or both.

D. Effect of Delay Dispersion

In the previous subsection, we chose f_{r} and T_{b} such that $\varphi \ll 1$ and $\varpi \ll 1$. To investigate the effect of delay dispersion, we fix the spreading factor and plot the average BER against different values of C_{D} and $\varphi = \varpi$ in Fig. 8. Note that for a fixed S, $\varphi = C_{\mathrm{D}}/S$ changes with C_{D}. Therefore, the curves are presented as functions of two parameters.

Let us first consider the simulation results. We observe a degraded performance at low and high values of C_{D}. A small C_{D} implies a small number of resolvable MPCs and therefore, a tap in deep fade has a strong negative influence on the average BER. As C_{D} increases, the link performance improves, but after a certain point, ISI and RD kick in which leads to performance deterioration. On the other hand, the curve for the semi-analytical results approaches the hardened channel case as C_{D} increases. This is because the results (39) were derived with the ISI- and RD-free assumption. In short, the figure indicates that although the FoTR system exploits channel diversity, the impairments from delay dispersion can shadow its advantages.

The curves indicate that the impairments (ISI and RD) kick in roughly at $\varphi = 0.025$. However, it is not clear at this point which of the two (ISI or RD) has a more pronounced impact. To understand this further, we fix C_{D}, and simulate the FoTR link for different values of f_{r} (and hence ϖ) in an ISI-free scenario. The ISI-free scenario is ensured by sending bits of the same polarity, i.e., $b_i = 1\ \forall i$. Since a large f_{r} implies a large operational bandwidth, the passband of the RFE filter is also accordingly adjusted. Fig. 9 illustrates the $\overline{\mathrm{BER}}$ against ϖ for a fixed $C_{\mathrm{D}} = 2$ and $\gamma = 22$ dB. A monotonic degradation in performance is observed as ϖ increases. This affirms our conclusions in Sec. III-B; RD always affect the performance, even in negligible ISI. The degraded link quality is a serious concern for MA, since the MA capability of FoTR relies on using different frequency offsets for different links [11].

In order to assess the penalty of using a large frequency offset on the received SNR per bit γ, we fix S and C_{D}, and simulate the FoTR link for different values of f_{r}. Fig. 10 and Fig. 11 illustrate the average BER as a function of γ for different values of $\varpi = f_{\mathrm{r}}\tau_{\mathrm{rms}}$. It is seen that for the given channel model, the penalty for a system using $\varpi = 0.1$ compared to a system with $\varpi = 0.01$ is around 2 dB, at an average BER of 10^{-3}. Secondly, the power penalty grows larger for each step increase in f_{r} (or ϖ); for instance, the penalty is a fraction of 1 dB between choosing $\varpi = 0.01$ and $\varpi = 0.03$, but it is more than 1 dB between choosing $\varpi = 0.07$ and $\varpi = 0.09$. Clearly, large values of f_{r} are not feasible. Therefore, f_{r} should be chosen such that the resulting power penalty can be supported by the link budget.

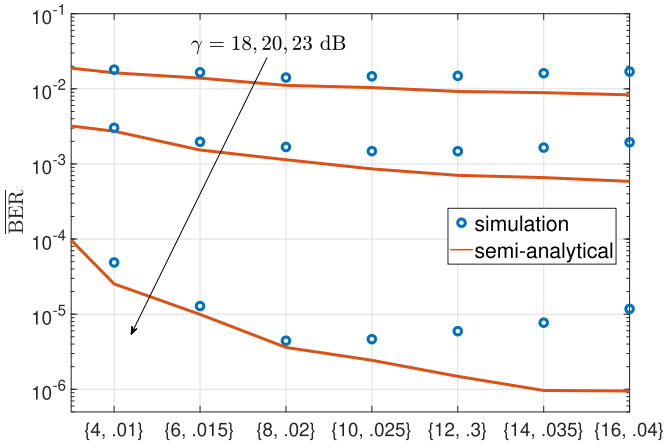

Fig. 8. $\overline{\mathrm{BER}}$ plotted against a combination of $C_{\mathrm{D}} = B_x\tau_{\mathrm{rms}}$ and $\varphi = \tau_{\mathrm{rms}}/T_{\mathrm{b}}$, for different values of γ and a fixed $S = 26$ dB.

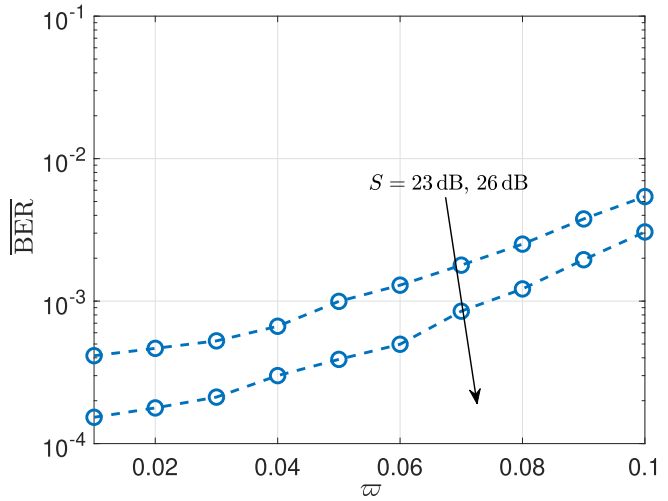

Fig. 9. $\overline{\mathrm{BER}}$ against increasing values of $\varpi = f_{\mathrm{r}}\tau_{\mathrm{rms}}$ in an ISI-free scenario.

For example, the penalty in required E_{b}/N_0 to achieve an average BER of 10^{-3} is less than 1 dB, as long as $\varpi \leq 0.05$.

DSP techniques can be employed to suppress RD and ISI. However, it increases the receiver complexity, which does not resonate with the design goals of FoTR. Therefore, one may carefully choose the system parameters such that ISI and RD are negligible. In this regard, we conclude from the observations in Fig. 8 till Fig. 11 that, as a guideline, one should choose the symbol rate such that $\varphi \leq 0.025$, and the frequency offset such that $\varpi \leq 0.05$. It must be stressed that the criteria are a rule-of-thumb, based on simulation results for a dense multipath channel that follows an exponential PDP. Therefore, the criteria can be different for different channel models and signaling schemes.[12]

Recall that in an MA scenario, each link is identified by a unique frequency offset $f_{\mathrm{r}} = c/T_{\mathrm{b}}$. If one employs the criterion $\varpi \leq 0.05$, one can solve that for a data rate of 10 kbps in an office environment ($\tau_{\mathrm{rms}} \approx 100$ ns), one can choose from a total of 40 available frequency offsets [23, p. 126]. This implies a possibility of maximum of 40 links in a network, in which all

[12]If a given data rate must be ensured, one can opt for higher-order modulation formats. Although they are less energy-efficient compared to BPSK, the criteria on φ and ϖ can be easier to meet.

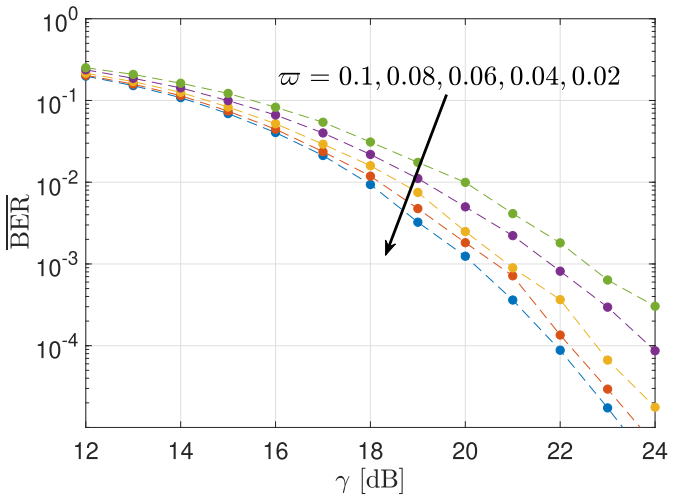

Fig. 10. Average BER versus $\gamma = E_\text{b}/N_0$ for a fixed $C_\text{D} = 4$, $S = 23$ dB, $\varphi \ll 1$, and different values of RD parameter ϖ.

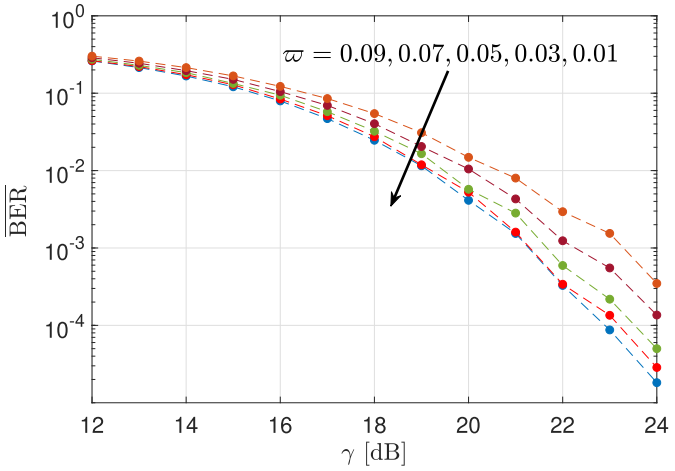

Fig. 11. Average BER versus $\gamma = E_\text{b}/N_0$ for a fixed $C_\text{D} = 4$, $S = 26$ dB, $\varphi \ll 1$, and different values of RD parameter ϖ.

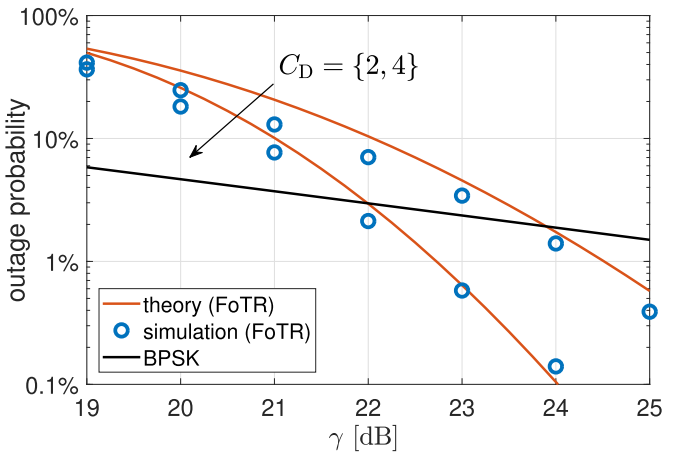

Fig. 12. Outage probability against $\gamma = E_\text{b}/N_0$ for different values of C_D, and a fixed $S = 23$ dB.

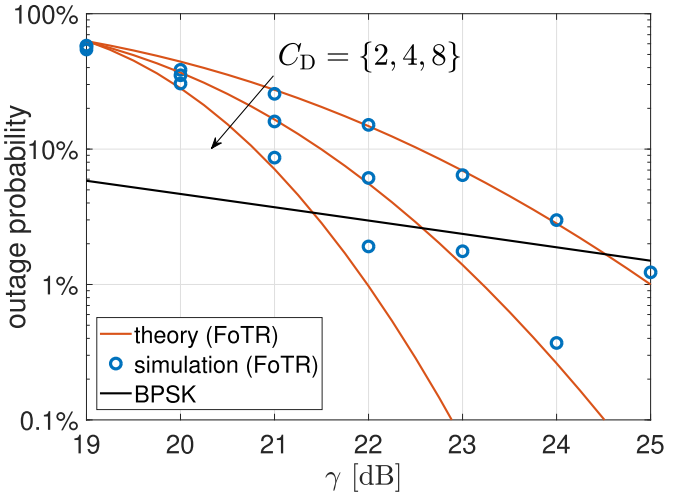

Fig. 13. Outage probability against $\gamma = E_\text{b}/N_0$ for different values of C_D, and a fixed $S = 26$ dB.

nodes see each other. For a large network, where the links in one cluster do not interfere with the links in another cluster, the frequency offsets can be reused.

E. Outage Probability

We now study the outage probability $\mathbb{P}_\text{out}$ of the FoTR link in dense fading channels. We consider the error threshold to be $\mathcal{E}_\text{T} = 10^{-3}$. In line with the earlier results, ISI and RD are ignored by choosing $\varphi = \varpi \ll 1$. For comparison, we also study the outage probability of a BPSK system, which can be shown to be $\mathbb{P}_\text{out} = 1 - \exp(-\Gamma_\text{T}/(2\gamma))$ [24].

In Fig. 12 and Fig. 13, we plot $\mathbb{P}_\text{out}$ against γ for two different values of S. First, we comment on the validity of the results. We observe that the theoretical and simulation results differ at high values of $\mathbb{P}_\text{out}$. This is likely due to the approximation $\beta_h \approx 2\alpha_h^2$ made in Sec. III-C. A high $\mathbb{P}_\text{out}$ corresponds to a high α_T, as seen from the expression in (44). Accordingly, a high $\mathbb{P}_\text{out}$ implies that the expression is evaluated for a large value of α_h. It was shown, with the help of Fig. 3, that the approximation is inaccurate for a large α_h, and more so, if S is small (large CNR). Nonetheless, high values of $\mathbb{P}_\text{out}$ are not interesting for the link design. In the region of significance ($1\% \leq \mathbb{P}_\text{out} \leq 10\%$), the difference in required γ for a certain $\mathbb{P}_\text{out}$ is a fraction of 1 dB.

The results indicate that one can achieve very low outage probabilities (1%) for an FoTR link in dense multipath fading channels. The channel diversity factor C_D plays an important role, and can significantly improve the required γ to achieve a certain $\mathbb{P}_\text{out}$. To investigate this further, we analyze γ_ρ, which as defined earlier, is the $\gamma = E_\text{b}/N_0$ required to remain below a tolerable level of the outage probability ρ. For $\mathcal{E}_\text{T} = 10^{-3}$ and $S = 23$ dB, γ_ρ is plotted against C_D in Fig. 14 for different values of ρ. As a reference, we also plot γ_ρ for BPSK, which can be shown to be

$$\gamma_\rho = -\Gamma_\text{T}/\big(2\log_e(1-\rho)\big).$$

We see that a high C_D reduces γ_ρ, but little gain is achieved beyond $C_\text{D} \geq 4$. In fact, for a very large C_D, the parameter γ_ρ attains an asymptote. This is a plausible result; for a fixed tolerable outage probability ρ, γ_ρ cannot be further reduced by improving the channel diversity factor. The lower

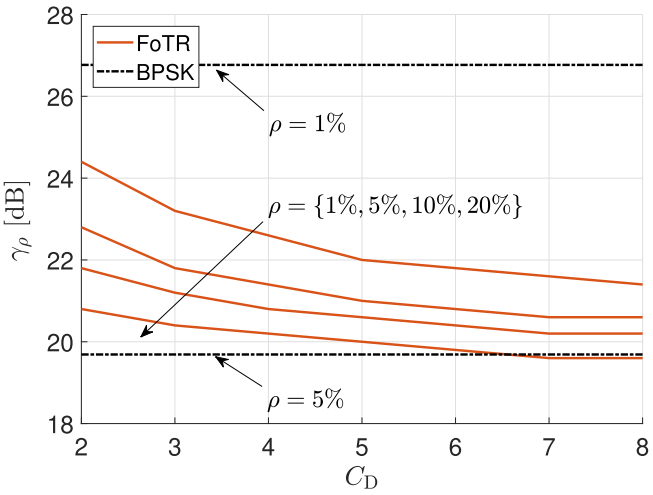

Fig. 14. Theoretical values of E_b/N_0, required to remain below an outage probability ρ, against increasing values of $C_\mathrm{D} = B_x \tau_\mathrm{rms}$.

bound on γ_ρ is imposed by the performance of the FoTR system in the hardened channel case. Therefore, γ_ρ in the figure asymptotically attains $18.5\,\mathrm{dB}$, for all values of ρ. Similarly, for $\mathcal{E}_\mathrm{T} = 10^{-6}$, γ_ρ would approach $24\,\mathrm{dB}$ for the chosen spreading factor. However, it must be stressed that the asymptotic value will not be achieved in practice. As C_D increases, the effect of delay dispersion will deteriorate the performance.

V. Conclusion

A wideband TR system, using frequency offset and a noise carrier, is studied in a dense multipath fading environment for its feasibility in low data rate sensor networks. A quasi-analytical expression for the BER is derived; the effect of delay dispersion and fading are investigated in relation with the key design parameters.

The delay dispersion not only leads to ISI, but also reference decoherence. A large frequency offset f_r implies dissimilar channel responses over the reference and information signals, and thus the signals lose coherence between them, leading to performance deterioration. For the studied channel and system model, it was found that choosing the symbol rate $1/T_\mathrm{b}$ and the frequency offset such that $\tau_\mathrm{rms}/T_\mathrm{b} \leq 0.025$ and $f_\mathrm{r}\tau_\mathrm{rms} \leq 0.05$ can ensure negligible impairments by delay dispersion. It was illustrated that these restrictions limit the data rate as well as the MA capability of the system. Therefore, FoTR can be used in those WSNs, where the overall offered traffic is low.

An approximated closed-form expression for the outage probability was also derived, which deviates from the simulation results by a fraction of $1\,\mathrm{dB}$ for low outage probabilities ($\mathbb{P}_\mathrm{out} \leq 10\%$). For an error threshold of 10^{-3} and the optimal spreading factor, it was found that FoTR can achieve less than 1% of outage probability for a nominal value of $\gamma = 23\,\mathrm{dB}$. Comparisons with a BPSK system suggest that, although FoTR suffers greatly from noise enhancement, it can be beneficial in multipath environments where outage probabilities of less than 5% are desired.

Appendix

In the appendix, we derive the noise powers Ψ_{yy}, Ψ_{yn}, and Ψ_{nn}, given in (25), that constitute the variance of the decision variable, given in (24).

A. Signal Self-Mixing Product

Using the definition of variance from (23), the noise contribution Ψ_{yy} is written as

$$\Psi_{yy} = \int_{-T_\mathrm{b}/2}^{T_\mathrm{b}/2}\int_{-T_\mathrm{b}/2}^{T_\mathrm{b}/2} C_{z_{yy}z_{yy}}(t_1,t_2)\,\mathrm{d}t_1\,\mathrm{d}t_2 = \int_{-T_\mathrm{b}/2}^{T_\mathrm{b}/2}\int_{-T_\mathrm{b}/2}^{T_\mathrm{b}/2} \cdot \Big(\mathbb{E}\big[z_{yy}(t_1)z_{yy}(t_2)\big] - \mathbb{E}\big[z_{yy}(t_1)\big]\mathbb{E}\big[z_{yy}(t_2)\big]\Big)\,\mathrm{d}t_1\,\mathrm{d}t_2. \quad (48)$$

The second term in the integrand can be solved similarly as in (19). Using the definition of $z_{yy}(t)$ from (14a), the first term in the integrand can be written as

$$\begin{aligned}&\int_{-T_\mathrm{b}/2}^{T_\mathrm{b}/2}\int_{-T_\mathrm{b}/2}^{T_\mathrm{b}/2} \mathbb{E}\big[z_{yy}(t_1)z_{yy}(t_2)\big]\,\mathrm{d}t_1\,\mathrm{d}t_2 \\ &= \frac{1}{64}\int_{-T_\mathrm{b}/2}^{T_\mathrm{b}/2}\int_{-T_\mathrm{b}/2}^{T_\mathrm{b}/2}\iiiint_{\mathcal{U}} \tilde{h}(u)\tilde{h}^*(v)\tilde{h}(w)\tilde{h}^*(s)a^2(t_1)a^2(t_2) \\ &\quad \cdot \mathbb{E}\big[\tilde{x}_g(t_1-u)\tilde{x}_g^*(t_1-v)\tilde{x}_g(t_2-w)\tilde{x}_g^*(t_2-s)\big] \\ &\quad \cdot \cos(2\pi f_\mathrm{r}t_1)\cos(2\pi f_\mathrm{r}t_2)\,\mathrm{d}u\,\mathrm{d}v\,\mathrm{d}w\,\mathrm{d}s\,\mathrm{d}t_1\,\mathrm{d}t_2, \end{aligned} \quad (49)$$

where for the brevity of notation, we have denoted $\iiiint_{\mathcal{U}}$ as a set of integral operations over the set of variables $\{u, v, w, s\}$ with limits $[-\infty, \infty]$. Using the moment theorem of complex Gaussian variables [25] in (49), and substituting the result in (48), it can be shown that

$$\begin{aligned}\Psi_{yy} &= \frac{1}{64}\int_{-T_\mathrm{b}/2}^{T_\mathrm{b}/2}\int_{t-T_\mathrm{b}/2}^{t+T_\mathrm{b}/2}\iiiint_{\mathcal{U}} \tilde{h}(u)\tilde{h}^*(v)\tilde{h}(w)\tilde{h}^*(s) \\ &\quad \cdot R_{\tilde{x}_g}(\tau+s-u)R^*_{\tilde{x}_g}(\tau+w-v)\,\mathrm{d}u\,\mathrm{d}v\,\mathrm{d}w\,\mathrm{d}s \\ &\quad \cdot a^2(t)\,a^2(t-\tau)\cos(2\pi f_\mathrm{r}t)\cos\big(2\pi f_\mathrm{r}(t-\tau)\big)\,\mathrm{d}\tau\,\mathrm{d}t,\end{aligned}$$

where we have substituted $\tau = t_1 - t_2$ and $t = t_1$. The support of the ACF $R_{\tilde{x}_g}(\tau)$ is very narrow ($\sim 1/B_x$). The narrowband terms, $a(t)$ and the cosines, hardly vary over the width of the ACF as well as the duration of $h(\tau)$. Therefore, we can approximate the above expression as

$$\begin{aligned}\Psi_{yy} &\overset{(a)}{\approx} \frac{1}{64}\int_{-\infty}^{\infty} S^2_{\tilde{x}_g}(f)\iiiint_{\mathcal{U}} \tilde{h}(u)\tilde{h}^*(v)\tilde{h}(w)\tilde{h}^*(s) \\ &\quad \cdot e^{j2\pi f(s-u+v-w)}\,\mathrm{d}u\,\mathrm{d}v\,\mathrm{d}w\,\mathrm{d}s\,\mathrm{d}f \\ &\quad \cdot \int_{-T_\mathrm{b}/2}^{T_\mathrm{b}/2} a^4(t)\cos^2(2\pi f_\mathrm{r}t)\,\mathrm{d}t \\ &\overset{(b)}{=} \frac{1}{64}\int_{-\infty}^{\infty} S^2_{\tilde{x}_g}(f)|\widetilde{H}(f)|^4\,\mathrm{d}f \int_{-T_\mathrm{b}/2}^{T_\mathrm{b}/2} a^4(t)\cos^2(2\pi f_\mathrm{r}t)\,\mathrm{d}t,\end{aligned}$$

where (a) follows from Plancherel's theorem and the Wiener-Kinchin relations; and (b) follows from the definition of Fourier transform. Substituting $a(t)$ from (5) and applying basic calculus and trigonometry, the integration over the

variable t solves to $25T_{\rm b}/16$ for a binary polar NRZ message signal and a frequency offset $f_{\rm r} = n/T_{\rm b}$. This results in

$$\begin{aligned}\Psi_{yy} &= \frac{25T_{\rm b}}{1024}\int_{-\infty}^{\infty} S_{\tilde{x}_g}^2(f)|\widetilde{H}(f)|^4\,{\rm d}f \\ &\overset{(a)}{=} \frac{25T_{\rm b}}{256}\cdot\left(\frac{P_x}{B_x}\right)^2\int_{-\infty}^{\infty}\mathcal{S}^4\left(\frac{f}{B_x}\right)|\widetilde{H}(f)|^4\,{\rm d}f \\ &\overset{(b)}{=} \frac{25\beta_h P_x^2 T_{\rm b}\lambda_2}{16L^2B_x},\end{aligned}$$

where (a) follows from (12a); and (b) follows from substituting $\nu = f/B_x$, and β_h from (27b).

B. Signal-Noise Mixing Product

The noise contribution from $z_{yn}(t)$ is solved as

$$\begin{aligned}\Psi_{yn} &= \int_{-T_{\rm b}/2}^{T_{\rm b}/2}\int_{-T_{\rm b}/2}^{T_{\rm b}/2} C_{z_{yn}z_{yn}}(t_1,t_2)\,{\rm d}t_1\,{\rm d}t_2 \\ &= \int_{-T_{\rm b}/2}^{T_{\rm b}/2}\int_{-T_{\rm b}/2}^{T_{\rm b}/2}\mathbb{E}\big[z_{yn}(t_1)z_{yn}(t_2)\big]\,{\rm d}t_1\,{\rm d}t_2,\end{aligned}$$

where the last equality follows because $z_{yn}(t)$ has a zero mean. Using the definition of $z_{yn}(t)$ from (14b), and using similar steps of derivation as in the last subsection, we get

$$\begin{aligned}\Psi_{yn} &\approx \frac{1}{16}\int_{-T_{\rm b}/2}^{T_{\rm b}/2} a^2(t)\cos^2(2\pi f_{\rm r}t)\,{\rm d}t \\ &\quad\cdot\int_{-\infty}^{\infty}\iint_{\mathcal{V}}\Big(\tilde{h}(u)\tilde{h}^*(v)R_{\tilde{x}_g}(\tau+v-u)R_{\tilde{n}_g}^*(\tau) \\ &\quad+\tilde{h}(v)\tilde{h}^*(u)R_{\tilde{x}_g}^*(\tau+v-u)R_{\tilde{n}_g}(\tau)\Big)\,{\rm d}u\,{\rm d}v\,{\rm d}\tau \\ &= \frac{1}{8}\int_{-T_{\rm b}/2}^{T_{\rm b}/2} a^2(t)\cos^2(2\pi f_{\rm r}t)\,{\rm d}t \\ &\quad\cdot\int_{-\infty}^{\infty} S_{\tilde{x}_g}(f)S_{\tilde{n}_g}(f)|\widetilde{H}(f)|^2\,{\rm d}f,\end{aligned}$$

where we have denoted $\iint_{\mathcal{V}}$ as a set of integral operations over the set of variables $\{u,v\}$ with limits $[-\infty,\infty]$. For the given signaling scheme, the integral over the variable t can be shown to be $5T_{\rm b}/8$. Using the definitions in (12), we can solve

$$\begin{aligned}\Psi_{yn} &= \frac{5T_{\rm b}}{16}\left(\frac{P_xN_0}{B_x}\right)\int_{-\infty}^{\infty}\mathcal{S}^3\left(\frac{f}{B_x}\right)|\widetilde{H}(f)|^2\,{\rm d}f \\ &= \frac{5\vartheta_h P_x T_{\rm b}N_0\lambda_1}{4L},\end{aligned}$$

where the last equality follows from substituting $\nu = f/B_x$, and ϑ_h from (27a).

C. Noise Self-Mixing Product

Using similar analysis, the noise contribution from $z_{nn}(t)$ in (14c) is solved to

$$\begin{aligned}\Psi_{nn} &= \int_{-T_{\rm b}/2}^{T_{\rm b}/2}\int_{-T_{\rm b}/2}^{T_{\rm b}/2}\mathbb{E}\big[z_{nn}(t_1)z_{nn}(t_2)\big]\,{\rm d}t_1\,{\rm d}t_2 \\ &\approx \frac{1}{4}\int_{-\infty}^{\infty}|R_{\tilde{n}_g}(\tau)|^2\,{\rm d}\tau\int_{-T_{\rm b}/2}^{T_{\rm b}/2}\cos^2(2\pi f_{\rm r}t)\,{\rm d}t \\ &= \frac{T_{\rm b}}{8}\int_{-\infty}^{\infty} S_{\tilde{n}_g}^2(f)\,{\rm d}f \\ &\overset{(a)}{=} \frac{1}{2}N_0^2T_{\rm b}\int_{-\infty}^{\infty}\mathcal{S}^2\left(\frac{f}{B_x}\right)\,{\rm d}f \\ &\overset{(b)}{=} \frac{1}{2}N_0^2B_xT_{\rm b},\end{aligned}$$

where (a) follows from (12b); and (b) follows from (2) and substitution of the variable $\nu = f/B_x$.

REFERENCES

[1] J. D. Choi and W. E. Stark, "Performance of ultra-wideband communications with suboptimal receivers in multipath channels," *IEEE J. Sel. Areas Commun.*, vol. 20, no. 9, pp. 1754–1766, Dec. 2002.

[2] B. L. Basore, "Noise-like signals and their detection by correlation," Ph.D. dissertation, Massachusetts Inst. Technol., Cambridge, MA, USA, May 1952.

[3] R. Hoctor and H. Tomlinson, "Delay-hopped transmitted-reference RF communications," in *Proc. IEEE Conf. Ultra Wideband Syst. Technol.*, Baltimore, MD, USA, May 2002, pp. 265–269.

[4] M. R. Casu, G. Durisi, and S. Benedetto, "On the implementation of a transmitted-reference UWB receiver," in *Proc. 13th Eur. Signal Process. Conf.*, Antalya, Turkey, Sep. 2005, pp. 1–4.

[5] A. A. D'Amico and U. Mengali, "Code-multiplexed UWB transmitted-reference radio," *IEEE Trans. Commun.*, vol. 56, no. 12, pp. 2125–2132, Dec. 2008.

[6] D. L. Goeckel, J. Mehlman, and J. Burkhart, "A class of ultra wideband (UWB) systems with simple receivers," in *Proc. IEEE Mil. Commun. Conf. (MILCOM)*, Orlando, FL, USA, Oct. 2007, pp. 1–7.

[7] K. Morrison, C. Capar, Z. Lai, D. Goeckel, and R. Jackson, "A unified framework for reference-based ultra-wideband signaling," in *Proc. IEEE Int. Conf. Ultra-Wideband*, Sep. 2009, pp. 290–294.

[8] J. Haartsen, X. Shang, J. W. Balkema, A. Meijerink, and J. L. Tauritz, "A new wireless modulation scheme based on frequency-offset," in *Proc. 12th Annu. Symp. IEEE/SCVT Benelux*, Enschede, The Netherlands, May 2005, pp. 1–7.

[9] D. L. Goeckel and Q. Zhang, "Slightly frequency-shifted reference ultra-wideband (UWB) radio: TR-UWB without the delay element," in *Proc. IEEE Mil. Commun. Conf.*, Atlantic City, NJ, USA, vol. 5, Oct. 2005, pp. 3029–3035.

[10] D. L. Goeckel and Q. Zhang, "Slightly frequency-shifted reference ultra-wideband (UWB) radio," *IEEE Trans. Commun*, vol. 55, no. 3, pp. 508–519, Mar. 2007.

[11] B. I. Bitachon, I. Bilal, A. Meijerink, and M. J. Bentum, "Near-far problem in noise-based frequency-offset modulation," in *Proc. 22nd Annu. Symp. IEEE/SCVT Benelux*, Luxembourg, Nov. 2015, pp. 1–6.

[12] Z. Lai, H. Joshi, D. Goeckel, D. Gupta, D. Gupta, and A. Mathew, "Performance of UWB systems in the presence of severe multipath and narrowband interference," in *Proc. IEEE Int. Conf. Ultra-Wideband*, Hannover, Germany, Sep. 2008, pp. 85–88.

[13] A. Meijerink and A. F. Molisch, "On the physical interpretation of the Saleh–Valenzuela model and the definition of its power delay profiles," *IEEE Trans. Antennas Propag.*, vol. 62, no. 9, pp. 4780–4793, Sep. 2014.

[14] D. Ye, R. van der Zee, and B. Nauta, "A 915 MHz 175 μW receiver using transmitted-reference and shifted limiters for 50 dB in-band interference tolerance," *IEEE J. Solid-State Circuits*, vol. 51, no. 12, pp. 3114–3124, Dec. 2016.

[15] I. Bilal, A. Meijerink, and M. J. Bentum, "Performance analysis of noise-based frequency offset modulation in dense frequency-selective fading channels," in *Proc. 9th ICSPCS*, Cairns, QLD, Australia, Dec. 2015, pp. 1–7.

[16] S. Haykin and M. Moher, *An Introduction to Analog and Digital Communications*. Hoboken, NJ, USA: Wiley, 2007.
[17] I. Bilal, A. Meijerink, and M. J. Bentum, "Optimum receiver filter for a noise-based frequency-offset modulation system," in *Proc. IEEE 27th Annu. Int. Symp. Pers., Indoor, Mobile Radio Commun. (PIMRC)*, Valencia, Spain, Sep. 2016, pp. 1–7.
[18] A. F. Molisch, *Wireless Communications*. Sussex, U.K.: Wiley, 2010.
[19] D. Horgan and C. C. Murphy, "On the convergence of the chi square and noncentral chi square distributions to the normal distribution," *IEEE Commun. Lett.*, vol. 17, no. 12, pp. 2233–2236, Dec. 2013.
[20] D. Cox, *Renewal Theory*. London, U.K.: Methuen, 1962.
[21] D. Hammarwall, M. Bengtsson, and B. Ottersten, "Acquiring partial CSI for spatially selective transmission by instantaneous channel norm feedback," *IEEE Trans. Signal Process.*, vol. 56, no. 3, pp. 1188–1204, Mar. 2008.
[22] J. C. Haartsen, A. Meijerink, A. Bekkaoui, A. Taban, and J. L. Tauritz, "Novel wireless modulation technique based on noise," in *Proc. 11th Annu. Symp. IEEE/SCVT Benelux*, Ghent, Belgium, Nov. 2004, pp. 1–8.
[23] S. Morshed, "Energy-efficient medium access control for transmit reference modulation," Ph.D. dissertation, Univ. Twente, Enschede, The Netherlands, Nov. 2017.
[24] U. Madhow, *Fundamentals of Digital Communication*. Cambridge, U.K.: Cambridge Univ. Press, 2008.
[25] I. Reed, "On a moment theorem for complex Gaussian processes," *IRE Trans. Inf. Theory*, vol. 8, no. 3, pp. 194–195, Apr. 1962.

Ibrahim Bilal was born in Pakistan, in 1986. He obtained M.Sc. degree from Royal Institute of Technology (KTH), Stockholm, Sweden in 2012, and his Ph.D. degree from the University of Twente, Enschede, the Netherlands in 2019.

From 2007 till 2010, he was employed at the cellular industry, establishing and maintaining cellular connectivity through optical fiber and microwave links. In 2012, he briefly worked as a research assistant in communication theory lab at KTH. He joined the Telecommunication Engineering Group at the University of Twente as a Ph.D. candidate in 2013. He was part of the research team working on the multi-disciplinary WALNUT project, where he explored the physical layer limitations of a frequency offset transmit-reference system. In November 2017, he was appointed as a lecturer at the university, and since August 2019, he has been working as a senior research engineer at Xsens B.V. in Enschede.

His research interests include channel and interference modeling, signal processing, sensor networks, and short-range communication techniques.

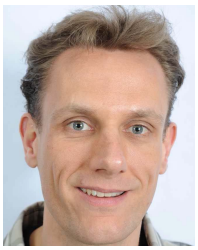

Arjan Meijerink (S'00–M'06–SM'11) was born in Almelo, the Netherlands, in 1976. He received the M.Sc. and Ph.D. degrees in Electrical Engineering (both with honors) from the University of Twente, Enschede, the Netherlands, in 2001 and 2005, respectively.

In 2000 he was a Trainee at Ericsson Business Mobile Networks in Enschede, developing error concealment techniques for Bluetooth voice links. From 2001 to 2005 he was a Research Assistant in the Telecommunication Engineering Group at the University of Twente, carrying out his Ph.D. research on optical coherence multiplexing. From 2005 to 2007 he was a Postdoctoral Researcher in the same group, working on RF photonic signal processing techniques, especially on the design and performance analysis of fully integrated ring resonator-based optical beamformers for wideband phased-array antenna systems. Since 2007 he has been an Assistant Professor in the Telecommunication Engineering Group, where he has been involved in research on new short-range radio transmission and localization techniques for wireless ad-hoc networks. In 2009 he was a Visiting Lecturer in the Wireless Communications Research Group at the Queen's University in Belfast, U.K., and in 2010 he was a Visiting Scholar in the Wireless Devices and Systems Group at the University of Southern California in Los Angeles, U.S.A. In 2019 he joined LioniX International B.V. in Enschede as an Integrated Optics Design Engineer.

Dr. Meijerink has published more than 70 papers in international journals, conferences and symposia. He is a member of the IEEE Communications Society and the International Union of Radio Science URSI, and has served as a reviewer for various journals, conferences and symposia. He was the Secretary of the IEEE Benelux Section from 2011 to 2013, and he was a Member of the Executive Committee of the IEEE Benelux Joint Chapter on Communications and Vehicular Technology from 2013 to 2017.

Mark J. Bentum (S'92–M'95–SM'09) was born in Smilde, The Netherlands, in 1967. He received the MSc degree in Electrical Engineering (with honors) from the University of Twente, Enschede, The Netherlands, in August 1991. In December 1995 he received the PhD degree for his thesis "Interactive Visualization of Volume Data" also from the University of Twente.

From December 1995 to June 1996 he was a research assistant at the University of Twente in the field of signal processing for mobile telecommunications and medical data processing. In June 1996 he joined the Netherlands Foundation for Research in Astronomy (ASTRON). He was in various positions at ASTRON. In 2005 he was involved in the eSMA project in Hawaii to correlate the Dutch JCMT mm-telescope with the Submillimeter Array (SMA) of Harvard University. From 2005 to 2008 he was responsible for the construction of the first software radio telescope in the world, LOFAR (Low Frequency Array). In 2008 he became an Associate Professor in the Telecommunication Engineering Group at the University of Twente. From December 2013 till September 2017 he was also the program director of Electrical Engineering at the University of Twente. In 2017 he became a Full Professor in Radio Science at Eindhoven University of Technology.

He is now involved with research and education in radio science. His current research interests are radio astronomy, short-range radio communications, novel receiver technologies (for instance in the field of radio astronomy), channel modeling, interference mitigation, sensor networks and aerospace. Prof. Bentum is a Senior Member of the IEEE, Chair of the IEEE Benelux section, initiator and chair of the IEEE Benelux AES/GRSS chapter, and has acted as a reviewer for various conferences and journals.